

*Bursts shape the NMDA-R mediated spike timing dependent plasticity curve: role of burst interspike interval and GABAergic inhibition*

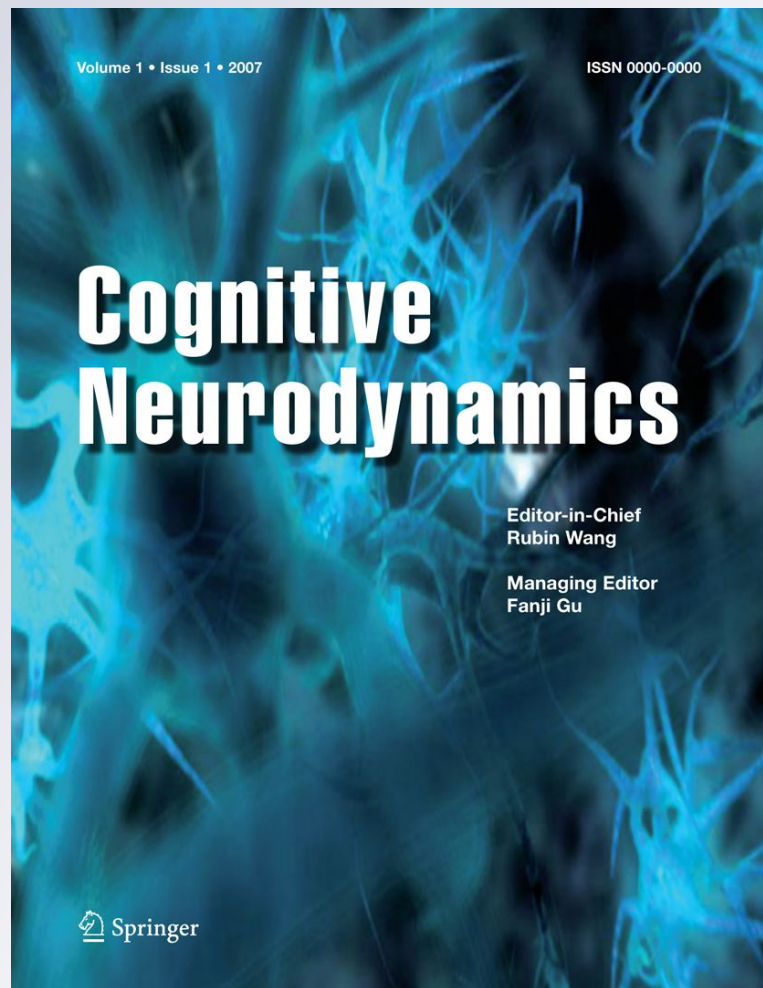
**Vassilis Cutsuridis**

**Cognitive Neurodynamics**

ISSN 1871-4080

Cogn Neurodyn

DOI 10.1007/s11571-012-9205-1



**Your article is protected by copyright and all rights are held exclusively by Springer Science+Business Media B.V.. This e-offprint is for personal use only and shall not be self-archived in electronic repositories. If you wish to self-archive your work, please use the accepted author's version for posting to your own website or your institution's repository. You may further deposit the accepted author's version on a funder's repository at a funder's request, provided it is not made publicly available until 12 months after publication.**

# Bursts shape the NMDA-R mediated spike timing dependent plasticity curve: role of burst interspike interval and GABAergic inhibition

Vassilis Cutsuridis

Received: 18 January 2012/Revised: 24 April 2012/Accepted: 2 May 2012  
© Springer Science+Business Media B.V. 2012

**Abstract** Spike timing dependent plasticity (STDP) is a synaptic learning rule where the relative timing between the presynaptic and postsynaptic action potentials determines the sign and strength of synaptic plasticity. In its basic form STDP has an asymmetric form which incorporates both persistent increases and persistent decreases in synaptic strength. The basic form of STDP, however, is not a fixed property and depends on the dendritic location. An asymmetric curve is observed in the distal dendrites, whereas a symmetrical one is observed in the proximal ones. A recent computational study has shown that the transition from the asymmetry to symmetry is due to inhibition under certain conditions. Synapses have also been observed to be unreliable at generating plasticity when excitatory postsynaptic potentials and single spikes are paired at low frequencies. Bursts of spikes, however, are reliably signaled because transmitter release is facilitated. This article presents a two-compartment model of the CA1 pyramidal cell. The model is neurophysiologically plausible with its dynamics resulting from the interplay of many ionic and synaptic currents. Plasticity is measured by a deterministic  $\text{Ca}^{2+}$  dynamics model which measures the instantaneous calcium level and its time course in the dendrite and change the strength of the synapse accordingly. The model is validated to match the asymmetrical form of STDP from the pairing of a presynaptic (dendritic) and postsynaptic (somatic) spikes as observed experimentally. With the parameter set unchanged the model investigates how pairing of bursts with single spikes and bursts in the presence or absence of inhibition shapes the STDP

curve. The model predicts that inhibition strength and frequency are not the only factors of the asymmetry-to-symmetry switch of the STDP curve. Burst interspike interval is another factor. This study is an important first step towards understanding how STDP is affected under natural firing patterns in vivo.

**Keywords** Computer model · Calcium · Theta burst · Inhibition · Backpropagating action potential · NMDA

## Introduction

In 1949 the Canadian psychologist Donald Hebb postulated that a synapse is strengthened only if the presynaptic and postsynaptic neurons are activated simultaneously (Hebb 1949). This postulate inspired many experimental neurophysiologists to investigate its cellular correlates, which led to the discovery of long-term potentiation (LTP) by Bliss and Lomo (1970) and long-term depression (LTD) by Stent (1973). The substrate for such synchronous firing in pre- and postsynaptic neurons was found to be the NMDA receptor, which acts as a coincidence detector. An NMDA receptor opens and allows  $\text{Ca}^{2+}$  to flow in only when presynaptic glutamate release is coincident with postsynaptic depolarization causing the removal of voltage-dependent magnesium block inside the NMDA channel pore (Mayer et al. 1984; Nowak et al. 1984). Strong activation of the NMDA receptor leading to a large  $\text{Ca}^{2+}$  influx at the postsynaptic site induces LTP, whereas weak NMDA receptor activation and moderate  $\text{Ca}^{2+}$  influx results in LTD (Bliss and Collingridge 1993).

Recently, Bi and Poo (1998) discovered that the relative timing between the pre- and postsynaptic action potentials determines the sign and amplitude of synaptic plasticity

---

V. Cutsuridis (✉)  
Division of Engineering, King's College London, Strand,  
London WC2R 2LS, UK  
e-mail: vcut@iit.demokritos.gr

(Bell et al. 1997; Bi 2002; Debanne et al. 1998; Magee and Johnston 1997; Markram et al. 1997; Sjöström et al. 2001; Yao and Dan 2001; Zhang et al. 1998). Bi and Poo (1998) also showed that the profile of the STDP curve in the in vitro hippocampal network has an asymmetrical shape with the largest LTP value at about +6 ms and the largest LTD value at about -10 ms. The area of the LTP region ( $\Delta\tau > 0$  ms) was shown to be smaller than the area of the LTD region ( $\Delta\tau < 0$  ms) (Bi and Poo 1998).

STDP has also been shown to depend on NMDA receptor activation and calcium influx through NMDAR channels (Caporale and Dan 2009; Markram et al. 1997; Sjöström et al. 2001). When an excitatory postsynaptic potential (EPSP) is generated before the generation of a postsynaptic action potential, then the synapse that transmitted the EPSP is potentiated, whereas when the EPSP arrives after the action potential generation, then the synapse is depressed. The synapse is informed that the neuron has generated an action potential by the arrival of the backpropagating action potential (Magee and Johnston 1997). Action potentials generated in the axon not only propagate along the axon towards presynaptic terminals, but are also capable of propagating backwards into the dendritic tree in many neurons (Stuart et al. 1997). There, they provide the necessary depolarization to relieve the  $Mg^{2+}$  block of the NMDA receptors, which is essential for STDP induction (Kampa et al. 2004; Vargas-Caballero and Robinson 2003). The timing of backpropagating action potentials relative to glutamate binding to NMDA receptors determines the amount of NMDA receptor activation and the  $Ca^{2+}$  influx (Koester and Sakmann 1998; Nevian and Sakmann 2004). Many computational models over the years modeled the postsynaptic  $Ca^{2+}$  in STDP and investigated what aspects of postsynaptic calcium serve as a plasticity signal and how postsynaptic calcium is used by other postsynaptic elements within the dendrite (Rubin et al. 2005; Karmarkar and Buonomano 2002; Abarbanel et al. 2003; Shouval et al. 2002; Bienstock et al. 1982).

STDP has been robustly observed in many species both in vivo and in vitro. Some of the excitatory glutamatergic synapses where STDP has been observed are found in: neurons in the visual cortex (Froemke and Dan 2002; Sjöström et al. 2001), neurons in the somatosensory cortex (Bender et al. 2006; Feldman 2000), neurons in the corticostriatum (Pawlak and Kerr 2008), cultured hippocampal neurons (Bi and Poo 1998), hippocampal CA3 neurons (Debanne et al. 1998), neurons in the dorsal cochlear neurons (Tzounopoulos et al. 2004), neurons in the retinotectal projection of the *Xenopus laevis* tadpole (Zhang et al. 1998) and neurons in the olfactory system of the locust *Schistocerca americana* (Cassenaer and Laurent 2007).

The shape of the STDP curve has been shown to be location dependent (Froemke et al. 2005). A recent experimental study has shown that when a pair of pulse stimuli was used to stimulate the stratum radiatum (SR) and the stratum oriens bordering the alveolar areas of a CA1 pyramidal cell, then the asymmetry of the STDP curve was not a fixed property, but as a matter of fact the shape of the STDP curve depended on the dendritic location of a CA1 pyramidal cell (PC). A symmetric STDP profile was observed in the proximal-to-the-soma dendrites, whereas an asymmetrical one was observed in the distal-to-the-soma dendrites (Aihara et al. 2007; Tsukada et al. 2005). Both experimental groups suggested that this transition from the symmetry to asymmetry is probably due to inhibition present in the CA1 PC dendrites, but they failed to show how and under what conditions this transition takes place.

In the hippocampus, inhibition comes in various frequencies (theta, gamma and ripples) and different phases with the ongoing network oscillations and inhibits distinct sub-cellular domains of pyramidal cells (PCs) (Cutsuridis et al. 2010b). Inhibitory interneurons entrain excitatory neurons to fire at different frequencies. Basket cells which target the soma and proximal dendrites of excitatory cells has been shown to phase spontaneous firing and sub-threshold oscillations in CA1 pyramidal cells at theta frequencies (Cobb et al. 1995), whereas OLM cells, which target the distal dendrites of CA1 and CA3 pyramidal cells, constitute an intrahippocampal mechanism for pacing nested gamma-theta rhythms in CA1 and CA3 regions (White et al. 2000). Networks of inhibitory interneurons have been shown to entrain hippocampal pyramidal cells at 40 Hz (Whittington et al. 1995). During gamma oscillations in vivo and in vitro, the different classes of interneurons fire action potentials at different phases with respect to the external oscillation and the firing of the pyramidal cells (Gloveli et al. 2010). Feedforward and feedback inhibition in region CA1 of the hippocampus has been shown to be a critical regulator of spike timing- and frequency-dependent plasticity (Nishiyama et al. 2010).

Cutsuridis et al. (2008, 2009b) and Cutsuridis (2011) was the first to quantitatively investigate via computer simulations the *inhibitory conditions* under which symmetry-to-asymmetry transition of the STDP curve occurs when a dendritic spike was paired with a somatic one at various interstimulus intervals. In these computational studies Cutsuridis et al. (2008, 2009b) investigated how STDP is shaped when presynaptic and postsynaptic action potentials (APs) are paired together in the presence of GABA inhibition, while varying the frequency of inhibition, its strength and its relative timing with the pre-post-synaptic excitatory stimulations. The central observation of the Cutsuridis (2011) study was that the STDP transition



from the symmetry to asymmetry is indeed due to inhibition as it has been suggested by the experimentalists (Aihara et al. 2007; Nishiyama et al. 2000; Tsukada et al. 2005). In addition Cutsuridis (2011) showed that (1) an inhibitory spike repeated every 250 ms (4 Hz) is *not* responsible for the asymmetry-to-symmetry transition, (2) an inhibitory burst repeated every 250 ms (4 Hz) (theta burst inhibition) is the necessary condition for the asymmetry-to-symmetry transition in the PC dendrite, (3) the transition depends on the strength of inhibition as well as on its relative presentation onset with the pre- and post-excitatory stimulation, (4) the asymmetry-to-symmetry transition appears only when the offset of the pre- and postsynaptic excitation coincides or partially overlaps with the onset of the inhibitory burst, (5) slow (50 Hz) and high (100 Hz) frequency inhibitory bursts repeated every 250 ms (4 Hz) have almost identical effects on the STDP asymmetry-to-symmetry transition when the pre- and postsynaptic excitation coincides or partially overlaps with the onset of the slow or fast inhibitory burst, (6) the LTP peak of the symmetric STDP curve was found to be centred at about  $\pm 10$  ms and not at 0 ms as it has been shown experimentally (Aihara et al. 2007; Tsukada et al. 2005), and (7) in contrast to experimental evidence (Aihara et al. 2007; Tsukada et al. 2005), two LTD windows are evident at about  $-10$  and  $+40$  ms and not at  $\pm 20$  ms.

Synapses of the CA1 PCs have been observed to be unreliable at signaling the arrival of single spikes to the postsynaptic neurons (Allen and Stevens 1994), thus making the pairing of excitatory postsynaptic potentials and single presynaptic APs ineffective at generating plasticity. In addition under certain experimental conditions single APs at the soma attenuate and hence fail to propagate to the dendrites (Jarsky et al. 2005; Stuart et al. 1997; Stuart and Hausser 2001). Thus, it was suggested that these failures can be addressed with high frequency AP bursts which will cause either effective AP backpropagation and generation of dendritic calcium spikes (Kampa and Stuart 2006; Larkum et al. 1999; Williams and Stuart 1999) or enhanced postsynaptic dendritic responses (Izhikevich et al. 2003; Lisman 1997; Paulsen et al. 1993). It has been shown that only bursts above a critical frequency ( $\sim 100$  Hz) of action potential firing induce dendritic spikes (Kampa and Stuart 2006; Larkum et al. 1999).

In contrast to Cutsuridis study (2011) where a pair of pulse stimuli were used to study how the shape of the STDP curve changes in the presence of inhibition, the scope of this paper is to understand how spike timing dependent synaptic plasticity is induced by natural firing patterns such as bursts, how this plasticity is affected when inhibition is present and how is the shape of STDP curve affected when bursts and inhibition interact in the dendrite of a CA1 pyramidal cell. To do so three stimulation protocols were employed: single

dendritic spikes paired with somatic bursts, dendritic burst paired with somatic spikes and dendritic bursts paired with somatic bursts. All three stimulation protocols were applied in the soma and dendrite of a CA1 pyramidal cell model (Cutsuridis 2011) both in the absence and presence of theta modulated inhibition. Because theta modulated slow (50 Hz) and high (100 Hz) frequency inhibitory bursts had computationally shown to have almost identical effects on the STDP asymmetry-to-symmetry transition (Cutsuridis 2011), then I chose for this study the theta modulated 100 Hz inhibition to be present with the pre- and postsynaptic excitatory pairings. Plasticity effects in the dendrite were measured via a biophysical mechanism based on a calcium detector system, which responded not only to calcium level (Karmarkar and Buonomano 2002; Abarbanel et al. 2003; Shouval et al. 2002), but also to  $\text{Ca}^{2+}$  temporal dynamics in the dendrite (Ismailov et al. 2004; Sabatini et al. 2001). This calcium detector system has been shown to yield a number of empirical findings from multi-spike experiments (e.g. pre-post LTP, post-pre LTD without a pre-post LTD window) (Rubin et al. 2005). The CA1 pyramidal cell model leads to a number of experimentally testable predictions that may lead to a better understanding of the STDP in the CA1 pyramidal cells of the hippocampus. Preliminary results of this research have been published previously in Cutsuridis (2010) and Cutsuridis et al. (2009a).

## Materials and methods

### The CA1 pyramidal cell model

The CA1 pyramidal cell model consists of two compartments: a soma and a dendrite (Fig. 1). The somatic compartment contains a sodium ( $\text{Na}^+$ ) current, a delayed rectifier  $\text{K}^+$  current, an A-type  $\text{K}^+$  current, a calcium-activated after-hyperpolarizing (AHP)  $\text{K}^+$  current and a HVA L-type  $\text{Ca}^{2+}$  current. The dendritic compartment contains a sodium ( $\text{Na}^+$ ) current, a delayed rectifier  $\text{K}^+$  current, an A-type  $\text{K}^+$  current and a HVA L-type  $\text{Ca}^{2+}$  current. AMPA, NMDA and  $\text{GABA}_A$  synapses are present only in the dendrite.

In the model, calcium enters the neuron through: (1) voltage-gated calcium channels (VGCCs), and (2) NMDA channels located at the SR dendrite. VGCCs are activated by the arrival of backpropagating action potentials (BPAPs) initiated in the soma by excitatory postsynaptic spikes. The NMDA channels are activated by the synergistic action of excitatory and inhibitory postsynaptic potentials and sufficient membrane potential depolarization due to the BPAP, which removes the magnesium block and allows calcium to enter the cell.

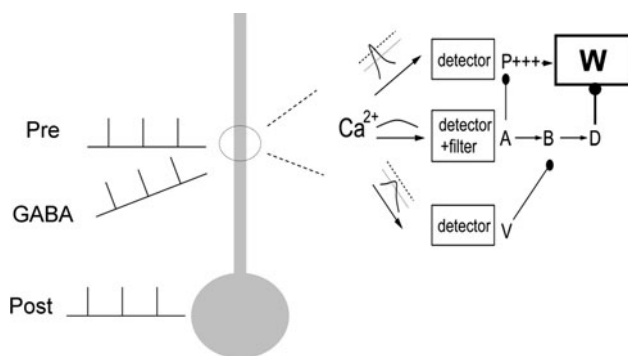


**Fig. 1** Our model CA1 neuron with its three transient inputs to the soma and dendrite. Synaptic plasticity at the dendritic synapses (circled region) is computed by a model detector system that responds to  $[Ca^{2+}]$  and produces an output of appropriate sign and magnitude. Three detector agents respond to the instantaneous  $[Ca^{2+}]$  in the model dendrite. Different calcium time courses lead to different time courses of the detectors  $P$ ,  $V$  and  $A$ . An intermediate element  $B$  is activated by  $A$ , while an additional agent  $D$  is activated by  $B$ , which is suppressed or vetoed by  $V$ .  $P$  and  $D$  then compete to influence the plasticity variable  $W$ , which serves as a measure of sign and magnitude of synaptic strength changes from the baseline.  $D$  acts as a filter to map  $[Ca^{2+}]$  time course onto  $W$

For a measure of plasticity a deterministic  $Ca^{2+}$  dynamics model is used (Bi and Rubin 2005; Rubin et al. 2005). The  $Ca^{2+}$  dynamics model consists of three detectors, which respond to the instantaneous calcium level and its time course in the dendrite and change the strength of the synapse accordingly (Fig. 1). More specifically, the detection system consists of: (1) a potentiation detector ( $P$ ), which detects calcium levels above a high-threshold ( $4 \mu M$ ) and triggers LTP, (2) a depression filter ( $D$ ), which detects calcium levels that exceed a low threshold level ( $0.6 \mu M$ ), remain above it for a minimum time period and trigger LTD, and (3) a veto

detector ( $V$ ), which detects levels exceeding a mid-level threshold ( $2 \mu M$ ) and triggers a veto of the model's depression components.

The detailed mathematical formalism of the model and its detector system can be found in the Appendix. The parameters of all ionic and synaptic currents used in the model are listed in Table 1. The parameters of the calcium detector system are listed in Table 2.

### Inputs

Two spike generators emulating the excitatory transient inputs to the soma and the dendrite were used to simulate the experimental STDP protocols. The burst generator (presynaptic (dendritic) or postsynaptic (somatic)) is given by

$$F_{burst}(t) = F_1(t) + F_2(t) + F_3(t) \tag{1}$$

where

$$F_1(t) = H(t-1) \cdot (H(\sin(2\pi \cdot (t-2)/T)) \cdot (1 - H(\sin(2\pi \cdot (t-1)/T))))$$

$$F_2(t) = H(t-1) \cdot (H(\sin(2\pi \cdot (t-2 - \text{int } bur)/T)) \cdot (1 - H(\sin(2\pi \cdot (t-1 - \text{int } bur)/T))))$$

and

$$F_3(t) = H(t-1) \cdot (H(\sin(2\pi \cdot (t-2 - 2 \cdot \text{int } bur)/T)) \cdot (1 - H(\sin(2\pi \cdot (t-1 - 2 \cdot \text{int } bur)/T))))$$

where  $\text{int } bur$  is the interspike interval with a burst,  $T$  is the period of oscillation and  $H()$  is the Heaviside function.

The spike generator (presynaptic (dendritic) or postsynaptic (somatic)) is given by

**Table 1** Parameter values of all ionic and synaptic currents

Symbol	Value	Symbol	Value	Symbol	Value	Symbol	Value
$g_L$	0.1	$g_{coup}$	1.125	$T$	23	$nonc$	6
$g_{Na,s}$	30	$V_{AMPA,NMDA}$	0	$\Delta\tau$	Variable	$asap$	0.001
$g_{Na,d}$	7	$V_{GABA}$	-75	$\Delta\tau_{GABA}$	Variable	$natt$	0
$g_{mAHP,s}$	25	$V_{Na}$	60	$period$	300	$qhat$	1
$g_{KA,s}$	75	$V_{Ca}$	140	$inact$	72	$s_1$	0
$g_{KA,d}$	12	$V_K$	-80	$inact_2$	0.11	$s_2$	40
$g_{Kdr,s}$	14	$V_L$	-70	$inact_3$	2	$s_3$	3.6
$g_{Kdr,d}$	0.867	$V_{Ca,NMDA}$	140	$inact_4$	64	$NMDA_{rate}$	2
$g_{CaLs}$	7	$\chi_{0,s}$	0.05	$inact_5$	1	$ndf$	10
$g_{CaLd}$	25	$\chi_{0,d}$	0.07	$\varphi_s$	0.1	$nds$	45
$g_{NMDA}$	0.3	$Ca_\tau$	1,000	$\varphi_d$	0.1	$buff$	0
$g_{AMPA}$	0.05	$Ca$	2	$\beta_s$	0.083	$\kappa$	7
$g_{Ca,NMDA}$	25	$Mg$	2	$\beta_d$	0.083	$\zeta_p$	30
$g_{GABA}$	0	$qmb$	0.28			$qma$	0.00048

**Table 2** Parameters in the calcium detector equations

Symbol	Value	Symbol	Value	Symbol	Value	Symbol	Value
$\alpha_w$	0.8	$\tau_A$	500	$\theta_c$	2 <sup>†</sup>	$num_b$	1
$\beta_w$	0.6	$\tau_B$	5	$\theta_d$	2.6	$num_c$	1
$a$	0.3	$\tau_C$	10	$\theta_e$	0.55	$num_d$	1
$d$	0.05	$\tau_D$	250	$\sigma_c$	-0.05	$num_e$	5
$p_a$	-0.1	$\tau_E$	40	$\sigma_d$	-0.01	$C_mHC$	4 <sup>†</sup>
$p_d$	-0.002	$c_p$	5	$\sigma_e$	-0.02	$C_mHN$	4
$\tau_w$	500	$c_d$	4	$num_a$	10	$C_nHC$	0.6 <sup>†</sup>
						$C_nHN$	3

<sup>†</sup> The sensitivity of the model was tested against a 10 % variation of these parameters. The model was shown to be robust against such variations

$$F_{spike}(t) = H(t - 1) \cdot (H(\sin(2\pi \cdot (t - 2 - \Delta\tau)/T)) \cdot (1 - H(\sin(2\pi \cdot (t - 1 - \Delta\tau)/T)))) \quad (2)$$

where  $\Delta\tau$  is the interval between the first spike of the burst and the spike (or the first spike of the second burst). In all experiments the pairing of the two excitatory inputs was repeated every 300 ms (3.5 Hz), typically for 5 s. The interstimulus interval  $\Delta\tau$  between the pre- and postsynaptic stimuli was variable ranging from -180 to 180 ms in increments of 5 ms, unless stated otherwise.

An inhibitory transient input to the dendrite was also used to investigate how GABA<sub>A</sub> modulates the NMDA-R mediated spike timing dependent plasticity. The dendritic GABAergic spike generator is given by

$$F_{GABA}(t) = \sum_{i=1}^{11} F_{GABA_i}(t) \quad (3)$$

where

$$F_{GABA_i}(t) = -aa_i \cdot H(t - 1) \cdot (H(\sin(2\pi \cdot (t - 2 + offset - (i - 1) \cdot \Delta\tau_{GABA})/T)) \cdot (1 - H(\sin(2\pi \cdot (t - 1 + offset - (i - 1) \cdot \Delta\tau_{GABA})/T))))$$

where *offset* is the relative timing between the onset of the GABA spike train and the pre-post interstimulus interval,  $\Delta\tau_{GABA}$  is the GABA interspike interval and  $aa_i$  is either 1 or 0 depending on the duration of the interval between the presynaptic and the postsynaptic stimuli (spikes or bursts) used.

### Experimental protocols

To investigate how the interaction of a burst with a spike or a burst with a burst in the presence or absence of inhibition modulated the NMDA-R spike timing dependent plasticity, I modelled six different experimental protocols in which the synaptic weight changed as a function of the presynaptic and postsynaptic spike statistics in the absence or presence of inhibition.

### Pairing of a dendritic burst and a somatic spike in the absence of inhibition

This protocol (see Fig. 4b) consisted of 16 sets of a dendritic burst and a somatic spike repeated every 300 ms (3.5 Hz) for about 5 s. The dendritic burst consisted of three spikes with variable interspike interval (ISI) (5 ms or 10 ms). Each pair was characterized by  $\Delta\tau = t_{postSpike} - t_{preBurst}$ , where  $t_{preBurst}$  is the first spike of the presynaptic (dendritic) burst and  $t_{postSpike}$  is the time of postsynaptic (somatic) spike.  $\Delta\tau$  was positive only when the dendritic burst preceded the somatic spike and negative when otherwise.

### Pairing of a dendritic burst and a somatic spike in the presence of GABA inhibition

In this inhibition protocol, an inhibitory spike train with 10 ms (100 Hz) interspike interval,  $\Delta\tau_{GABA}$ , was repeated every 300 ms (3.5 Hz) for about 5 s (a total of 16 spike trains). Each inhibitory spike train was bounded by the onset and offset of the dendritic burst-somatic spike stimulation (see Fig. 4c).

### Pairing of a dendritic spike and a somatic burst in the absence of inhibition

This protocol (see Fig. 10b) consisted of 16 sets of a dendritic spike and a somatic burst repeated every 300 ms (3.5 Hz) for about 5 s. The somatic burst consisted of three spikes with variable interspike interval (ISI) (2 ms or 5 ms or 10 ms). Each pair was characterized by  $\Delta\tau = t_{postBurst} - t_{preSpike}$ , where  $t_{postBurst}$  is the first spike of the postsynaptic (somatic) burst and  $t_{preSpike}$  is the time of presynaptic (dendritic) spike.  $\Delta\tau$  was positive only when the dendritic spike preceded the somatic burst and negative otherwise.

### Pairing of a dendritic spike and a somatic burst in the presence of GABA inhibition

In this inhibition protocol, an inhibitory spike train with 10 ms (100 Hz) interspike interval,  $\Delta\tau_{GABA}$ , was repeated

every 300 ms (3.5 Hz) for about 5 s (a total of 16 spike trains). Each inhibitory spike train was bounded by the onset and offset of the dendritic spike-somatic burst stimulation (see Fig. 10c).

*Pairing of a dendritic burst and a somatic burst in the absence of inhibition*

This protocol (see Fig. 14b) consisted of 16 sets of a dendritic burst and a somatic burst repeated every 300 ms (3.5 Hz) for about 5 s. Each somatic and dendritic burst consisted of three spikes with variable interspike interval (ISI) (2 ms or 5 ms). Each pair was characterized by  $\Delta\tau = t_{\text{postBurst}} - t_{\text{preBurst}}$ , where  $t_{\text{postBurst}}$  is the first spike of the postsynaptic (somatic) burst and  $t_{\text{preBurst}}$  is the time of presynaptic (dendritic) burst.  $\Delta\tau$  was positive only when the dendritic burst preceded the somatic burst and negative otherwise.

*Pairing of a dendritic burst and a somatic burst in the presence of GABA inhibition*

In this inhibition protocol, an inhibitory spike train with 10 ms (100 Hz) interspike interval,  $\Delta\tau_{\text{GABA}}$ , was repeated every 300 ms (3.5 Hz) for about 5 s (a total of 16 spike trains). Each inhibitory spike train was bounded by the onset and offset of the dendritic burst-somatic burst stimulation (see Fig. 14c).

Implementation

All simulations were performed using the software XPPAUT (Ermentrout 2002). A fourth order Runge–Kutta method was used for numerical integration in XPPAUT

with a step size of  $\delta t = 0.075$  ms. The MATLAB graphics toolbox was used for visualization of the simulation results. The implementation code of the model is available upon request.

Results

Model validation: pairing of presynaptic (dendritic) and postsynaptic (somatic) spikes in the absence of inhibition

When a presynaptic (dendritic) spike is paired with a postsynaptic (somatic) spike in the absence of inhibition then an asymmetric STDP curve appears with the largest LTP and LTD values at +5 ms and at -10 ms, respectively (Bi and Poo 1998). The saturated synaptic weight values ( $W_{\infty}$ ) as a function of the interstimulus interval,  $\Delta\tau = t_{\text{post}} - t_{\text{pre}}$  are depicted in Fig. 2.  $\Delta\tau$  is the interstimulus interval between the presynaptic dendritic spike and the postsynaptic somatic spike. For each  $\Delta\tau$ , the pre- and postsynaptic pairing was repeated every 300 ms (3.5 Hz) until saturation, typically for 5 s.  $W_{\infty}$  is measured as the saturated value of the readout variable  $W$  at  $t = 5$  s. In the case where the saturated  $W$  is oscillating between two values,  $W_{\infty}$  is the mean value of these two values. Simulations were performed with  $\Delta\tau$  ranging from -100 to 100 ms in increments of 5 ms. The area of the LTP region ( $\Delta\tau > 0$ ) is smaller than the area of the LTD region ( $\Delta\tau < 0$ ), as it has been experimentally observed (Bi and Poo 1998). At interstimulus intervals  $\Delta\tau > +40$  ms and  $\Delta\tau < -70$  ms  $W_{\infty}$  approaches zero.

In the paired pre-10-post stimulation protocol, where a presynaptic (dendritic) stimulation is followed 10 ms later

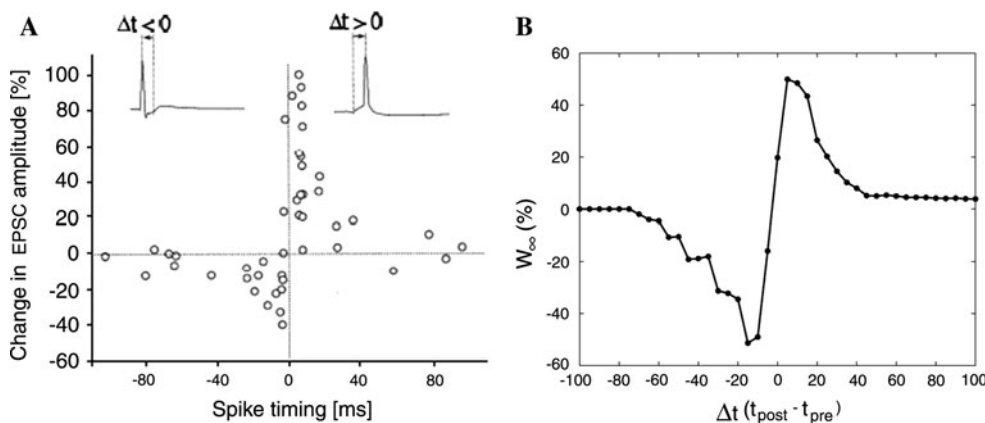
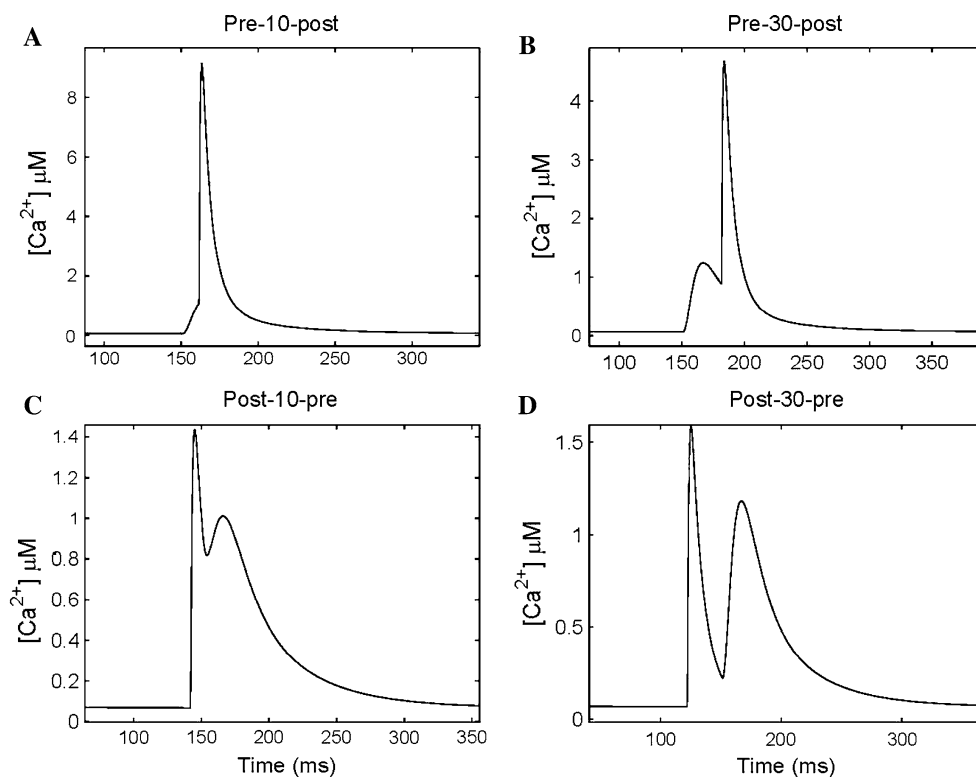


**Fig. 2** **a** Experimentally observed STDP curve as a function of spiking timing. Spike timing was defined as the time interval between the onset of the EPSP and the peak of the postsynaptic action potential during each cycle of repetitive stimulation (reprinted with permission from Bi and Poo 1998). **b** Simulated STDP curve from spike pair

simulations in the absence of GABA<sub>A</sub>.  $W_{\infty}$  is the saturated value of the readout variable  $W$  (see Fig. 1) measured at the end of each simulation run multiplied by 100 (%).  $\Delta\tau (t_{\text{post}} - t_{\text{pre}})$  ranges from -100 to 100 ms in increments of 5 ms



**Fig. 3** Postsynaptic calcium time courses in the absence of GABA<sub>A</sub>. Times shown are measured relative to the onset of the stimulation experiments. **a** Pre-10-post case. **b** Pre-30-post case. **c** Post-10-pre case. **d** Post-30-pre case



by a postsynaptic (somatic) stimulation, a large calcium influx through the NMDA channels is evident in the SR dendrite due to the removal of the magnesium block by the BPAP (Fig. 3a). In the pre-30-post scenario, 30 ms after the presynaptic (dendritic) stimulation a BPAP will arrive at the dendrite causing removal of the magnesium block from the NMDA channels. By then though more and more NMDA channels will be inactivated and hence the calcium influx will be greatly reduced (compare peak calcium level in Fig. 3a, b). The peak calcium level will continue to decrease as the pre-post interstimulus interval is lengthened.

In the post-10-pre scenario (see Fig. 3c), the calcium influx is once again greatly reduced due to a different time course than in the pre-30-post case. This time most of the calcium comes through the VGCCs producing a slight amplitude increase in calcium influx almost immediately, followed by a second calcium with a lower peak. The valley that separates the two peaks is above the 0.6  $\mu\text{M}$  threshold, but below the 2  $\mu\text{M}$  threshold, which triggers the depression (D) detector, but not the veto (V) detector and produces LTD. In the post-30-pre case, the two calcium level peaks are more distinguishable, because of the 30 ms delay between the post stimulation and the pre-stimulation (see Fig. 3d). The valley that separates them drops below the 0.6  $\mu\text{M}$  threshold causing a much smaller LTD. The results summarized in this section have been published before in Cutsuridis (2011). The parameter set used to

reproduce the results in this section was used to reproduce the results in the following sections.

Pairing of a dendritic burst and a somatic spike in the absence of inhibition (Fig. 4)

The saturated synaptic weight values ( $W_{\infty}$ ) at the dendrite as a function of the interstimulus interval,  $\Delta\tau = t_{\text{post}} - t_{\text{pre}}$ , and burst interspike interval (bISI) are depicted in Fig. 5. In this case,  $\Delta\tau$  is the interstimulus interval between the first spike of the presynaptic dendritic burst and the postsynaptic somatic spike. For each  $\Delta\tau$  the pre- and postsynaptic pairing is repeated every 300 ms (3.5 Hz) until saturation, typically for 5 s. As before  $W_{\infty}$  is measured at the saturated value of the readout variable  $W$  at  $t = 5$  s. When the saturated  $W$  is oscillating between two values, then  $W_{\infty}$  is the mean of these two values. Simulations were performed with  $\Delta\tau$  ranging from  $-180$  to  $180$  ms in increments of 5 ms. An asymmetric STDP curve is shown with the largest LTP and LTD values at  $+15$  ms and at  $-5$  ms, respectively, when bISI is 5 ms. As bISI is increased to 10 ms, the asymmetric STDP curve remains asymmetric, but shifts to the right with the peak LTP value increased by 0.14 units and at  $+40$  ms and the lowest LTP value increased by 0.1 units and set at 0 ms. The STDP curve levels off at 0.4 units and never decays back to zero even at  $\Delta\tau = \pm 180$  ms. This is due to the repetition period of the pre-postsynaptic excitatory stimulation (every

**Fig. 4** **a** Our model CA1 neuron with its three transient inputs to the soma and dendrite. Inputs: an excitatory burst to the dendrite, an excitatory spike to the soma and an inhibitory spike to the dendrite. Each input repeats every 300 ms for about 5 s. **b** Pairing of a dendritic burst with a somatic spike in the absence of inhibition. **c** Pairing of a dendritic burst with a somatic spike in the presence of GABA inhibition

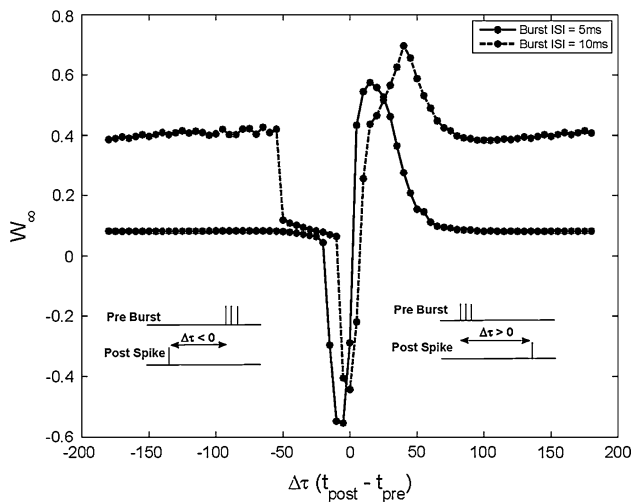
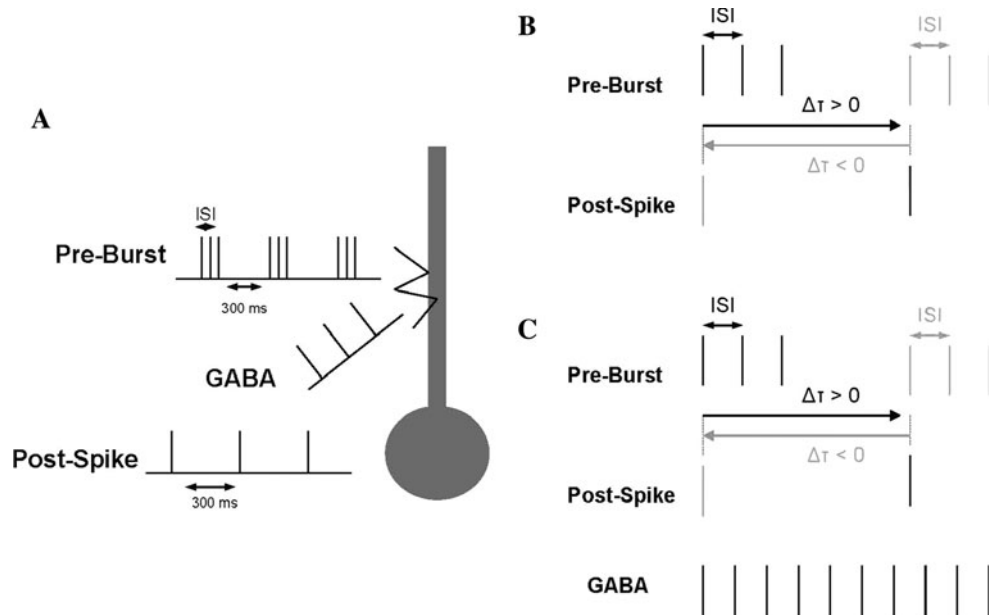


**Fig. 5** Simulated STDP profile as a function of burst interspike interval (burst ISI) in the absence of inhibition.  $\Delta\tau$  ( $t_{\text{post}} - t_{\text{pre}}$ ) is the interstimulus interval between the first spike of the dendritic burst and the somatic spike.  $\Delta\tau$  ranges from  $-180$  to  $180$  ms in increments of  $5$  ms. (Inset—left) PostSpike–PreBurst scenario, where somatic single spike precedes the dendritic burst, comprised of three spikes, by  $\Delta\tau$ .  $\Delta\tau$  takes values from  $-5$  to  $-180$  ms in increments of  $5$  ms. The pairing repeats every  $300$  ms for about  $5$  s. (Inset-right) PreBurst–PostSpike scenario, where a dendritic burst precedes the somatic spike by  $\Delta\tau$ .  $\Delta\tau$  takes values from  $0$  to  $+180$  ms in increments of  $5$  ms. The pairing repeats every  $300$  ms for about  $5$  s

$300$  ms), which allows the effects of the postsynaptic spike at  $\Delta\tau > 150$  ms to interact with the effects of the presynaptic burst at the start of next pre-post excitatory stimulation.

In the preBurst-( $40$  ms)-postSpike case, the peak LTP value when the bISI is  $5$  ms is approximately at  $0.27$ , whereas when the bISI is  $10$  ms, the peak LTP value is  $0.7$

(see Fig. 6b). This increase in potentiation (see Fig. 6c) is due to a larger amount of  $\text{Ca}^{2+}$  influx through the NMDA channel when bISI is  $10$  ms, thus allowing the time course of its concentration to stay above the  $2 \mu\text{M}$  (veto threshold) and the  $4 \mu\text{M}$  (potentiation threshold) a longer period of time (approximately  $70$  ms) (see Fig. 6a). In the case of bISI at  $5$  ms, the calcium influx through the NMDA channel is greatly reduced, followed by a second calcium pulse with a higher peak  $40$  ms after the burst. The NMDA calcium pulse stays above the  $2 \mu\text{M}$  veto threshold for a small period of time (approximately  $10$  ms) and subsequently decays to values below this threshold, thus triggering for  $2$ – $3$  ms the depression (D) detector, which counteracts any previously triggered potentiation. The D response is very brief and it is followed by a calcium influx through the VGCC, which cause a second calcium pulse to peak above the  $4 \mu\text{M}$  threshold, which re-potentiates the synapse and causes the synaptic weight to saturate to  $0.27$  units (see Fig. 6b).

In the postSpike-( $-10$  ms)-preBurst case, the calcium influx is greatly reduced due to a different time course than in the previous case. The first calcium spike comes from the VGCC and peaks under the  $2 \mu\text{M}$  threshold, thus triggering the depression (D) detector (see Fig. 7d). The second calcium spike comes from the NMDA channels at the dendrite which opened by the dendritic burst. When bISI is  $5$  ms, the second calcium spike peaked and stayed above the  $2 \mu\text{M}$  threshold for less than  $5$  ms and then decayed to zero. When bISI is  $10$  ms the second calcium spike peaked at  $2.5 \mu\text{M}$  and stayed above the  $2 \mu\text{M}$  threshold for a longer period of time, thus triggering a larger veto response than before (compare veto pulses from Figs. 7d, e). I remind the reader that the veto (V) response

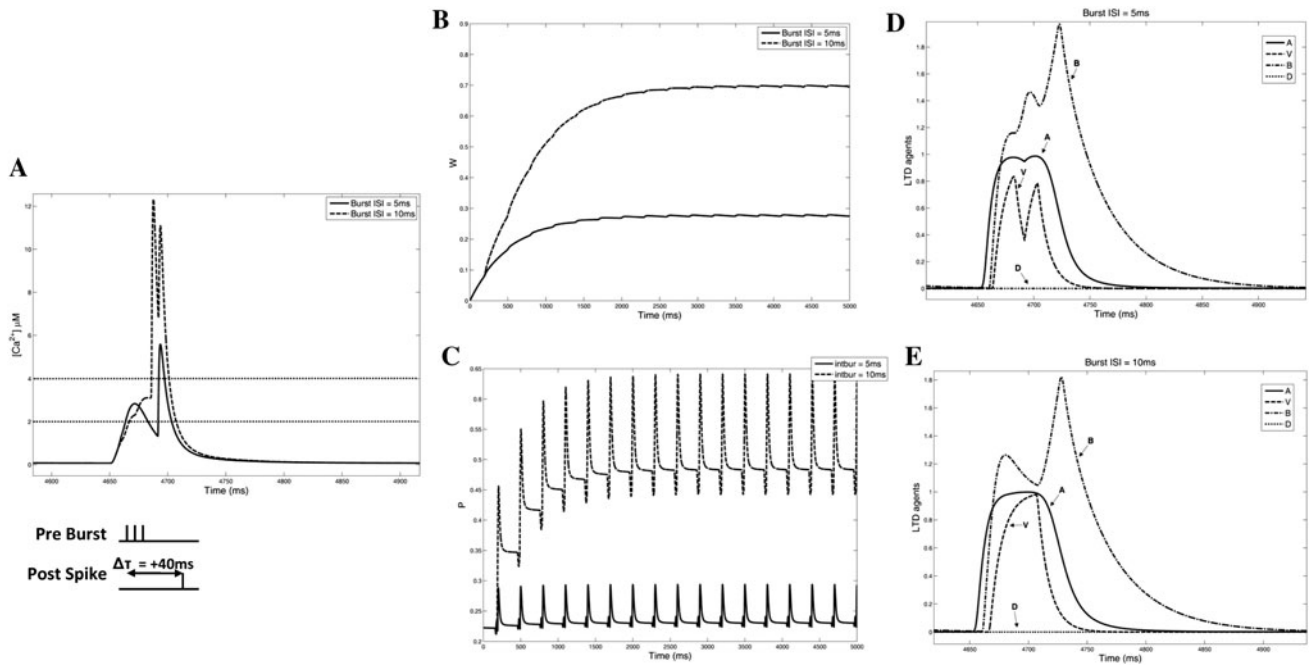


**Fig. 6** **a** *Bottom*: Graphical representation of preBurst-(+40 ms)-postSpoke stimulation paradigm in the absence of GABA inhibition. *Top*: Time course of  $Ca^{2+}$  concentration ( $\mu M$ ) as a function of burst interspike intervals (ISIs) (5 and 10 ms) in the absence of GABA inhibition in the preBurst-(+40 ms)-postSpoke scenario. **b** Time course of synaptic weight ( $W$ ) as a function of burst interspike intervals (ISIs) (5 and 10 ms) without GABA inhibition in the preBurst-(+40 ms)-postSpoke scenario. **c** Time course of potentiation

( $P$ ) as a function of burst interspike intervals (ISIs) (5 and 10 ms) without GABA inhibition in the preBurst-(+40 ms)-postSpoke scenario. **d** Time course of LTD agents ( $A$ ,  $B$ ,  $V$ , and  $D$ ) in the absence of inhibition in the preBurst-(+40 ms)-postSpoke scenario when burst ISI is 5 ms. **e** Time course of LTD agents ( $A$ ,  $B$ ,  $V$ , and  $D$ ) in the absence of inhibition in the preBurst-(+40 ms)-postSpoke scenario when burst ISI is 10 ms

inhibits and counteracts the response of the depression ( $D$ ) detector. Hence, the  $D$  response is larger in the 5 ms bISI case than in the 10 ms bISI one. Thus, the synaptic weight ( $W$ ) saturates to a positive value when bISI is 10 ms and to a negative one when bISI is 5 ms (see Fig. 7b).

Pairing of a dendritic burst and a somatic spike in the presence of an 100 Hz inhibitory spike train as a function of GABA conductance and burst interspike interval

As GABA inhibition is increased, then the shape of the STDP curve transitions from asymmetry to symmetry (see Fig. 8). When  $g_{GABA}$  is 0.1 mS/cm<sup>2</sup>, then the shape of the STDP curve resembles a Mexican hat consisting of a peak positive phase at +10–15 ms when bISI is 5 ms and +10 ms when bISI is 10 ms and two peak negative regions at –5 ms and +65 ms when bISI is 5 ms and at –5 ms and +80 ms when bISI is 10 ms. As  $g_{GABA}$  increases (0.2 mS/cm<sup>2</sup>), then the shape of the STDP curve is a fully symmetrical one with flat negative tails and a single positive region. It has been shown that the symmetrical STDP profile with short temporal windows may serve as a coincidence detector between the input and the output and may

play a role in the heteroassociation of memories (Cutsuridis et al. 2010a, 2011; Cutsuridis and Wennekers 2009), whereas an asymmetric STDP profile with broad temporal windows may play a role in the temporal chunking of memories (Hayashi and Igarashi 2009). When bISI is 5 ms, then the peak LTP value is slightly reduced as  $g_{GABA}$  is increased, but the peak LTD value remains unaffected (see Fig. 8a). Similarly, when bISI is 10 ms, then the peak LTP value is slightly reduced as  $g_{GABA}$  increases and is shifted rightwards by about 15 ms. A similar reduction is observed for the peak LTD value when  $g_{GABA}$  increases (see Fig. 8b).

Figure 9 depicts the time courses of  $Ca^{2+}$  and LTD agents in the peak LTP and LTD values as  $g_{GABA}$  increases. In the preBurst-(+40 ms)-postSpoke case (see Fig. 9A1), the peak of the calcium spikes (VGCC and NMDA) are greatly reduced as  $g_{GABA}$  increases. The VGCC calcium spikes peak just above the 4  $\mu M$  threshold, but stay over for a small period of time before decaying to zero. Because the  $B$  agents when  $g_{GABA}$  is 0.1 and 0.2 mS/cm<sup>2</sup> is well under the 2.5 threshold (see Fig. 9A2), then the depression ( $D$ ) response is zero. Similarly in the postSpoke(–10 ms)-preBurst case (see Fig. 9B1), the time course of the NMDA and VGCC calcium fluxes are most of the time below the

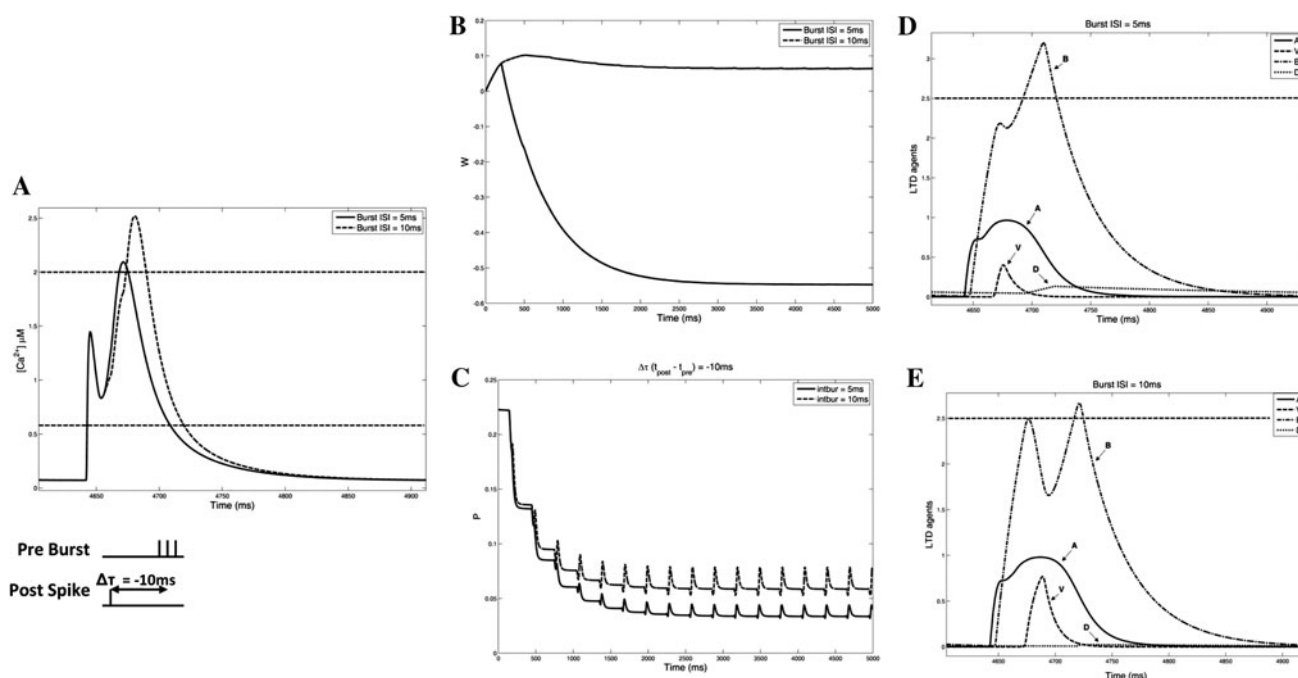


**Fig. 7 a Bottom:** Graphical representation of postSpike(-10 ms)-preBurst stimulation paradigm in the absence of GABA inhibition. **Top:** Time course of  $Ca^{2+}$  concentration ( $\mu M$ ) as a function of burst interspike intervals (ISIs) (5 and 10 ms) in the absence of GABA inhibition in the postSpike(-10 ms)-preBurst scenario. **b** Time course of synaptic weight ( $W$ ) as a function of burst interspike intervals (ISIs) (5 and 10 ms) without GABA inhibition in the postSpike(-10 ms)-preBurst scenario. **c** Time course of potentiation

( $P$ ) as a function of burst interspike intervals (ISIs) (5 and 10 ms) without GABA inhibition in the postSpike(-10 ms)-preBurst scenario. **d** Time course of LTD agents ( $A$ ,  $B$ ,  $V$ , and  $D$ ) in the absence of inhibition in the postSpike(-10 ms)-preBurst scenario when burst ISI is 5 ms. **e** Time course of LTD agents ( $A$ ,  $B$ ,  $V$ , and  $D$ ) in the absence of inhibition in the postSpike(-10 ms)-preBurst scenario when burst ISI is 10 ms

2  $\mu M$  threshold and hence the responses of the D detectors are larger (compare Fig. 9A2, B2). The NMDA  $Ca^{2+}$  fluxes when  $g_{GABA}$  is 0.1 and 0.2 mS/cm<sup>2</sup> barely peak above the 2  $\mu M$  threshold and hence their veto responses are smaller than in 0 mS/cm<sup>2</sup> case (see Fig. 9B1).

Pairing of a dendritic spike and a somatic burst in the absence of inhibition (see Fig. 10a, b)

The saturated synaptic weight values ( $W_{\infty}$ ) at the dendrite as a function of interstimulus interval,  $\Delta\tau$ , and bISI are depicted in Fig. 11. In this case where a dendritic spike is paired with a somatic burst, the interstimulus interval  $\Delta\tau$  is defined as the interval between the dendritic spike and the first spike of the somatic burst. As before, for each  $\Delta\tau$ , the pre- and postsynaptic pairing was repeated every 300 ms (3.5 Hz) until saturation, for about 5 s.  $\Delta\tau$  varied from -180 to 180 ms in increments of 5 ms.  $W_{\infty}$  was the saturated synaptic weight value  $W$  at 5 s. A fully symmetric STDP curve with flat LTD tails is shown with the peak LTP value at 0-5 ms. As bISI increases from 2 to 10 ms, the peak LTP value increases by a factor of 0.15 units. This happens because as the burst ISI increases the  $Ca^{2+}$  influx peaks not once but twice, thus making the area under the

$Ca^{2+}$  curve broader and the  $Ca^{2+}$  time course longer (see Fig. 12a). These increases result in a lightly higher veto response and smaller peaked B agent response when bISI is 5 ms (see Figs. 12b, c). Thus, the potentiation ( $P$ ) response when bISI is 5 ms is greater than when bISI is 2 ms (data not shown).

Pairing of a somatic burst and a dendritic spike in the presence of an 100 Hz inhibitory spike train as a function of GABA conductance and burst interspike interval (see Fig. 10a, c)

In the presence of inhibition many interesting findings are evident (see Fig. 13). As  $g_{GABA}$  is increased, then the shape of the STDP curve transition from symmetry with flat LTD tails when  $g_{GABA}$  is 0.0 mS/cm<sup>2</sup> to Mexican hat shaped symmetry. When bISI is 2 ms, the peak LTD values are at +40 and -10 ms, but when bISI is 5 ms LTD peaks at -15 and +50-60 ms. The peak LTP value is reduced by equal amounts as  $g_{GABA}$  is increased. The latter is because inhibition hyperpolarizes the membrane potential bringing it to values away from the spiking threshold, thus strengthening the voltage-dependent  $Mg^{2+}$  block of NMDAR, which leads to lower  $Ca^{2+}$  influx through the

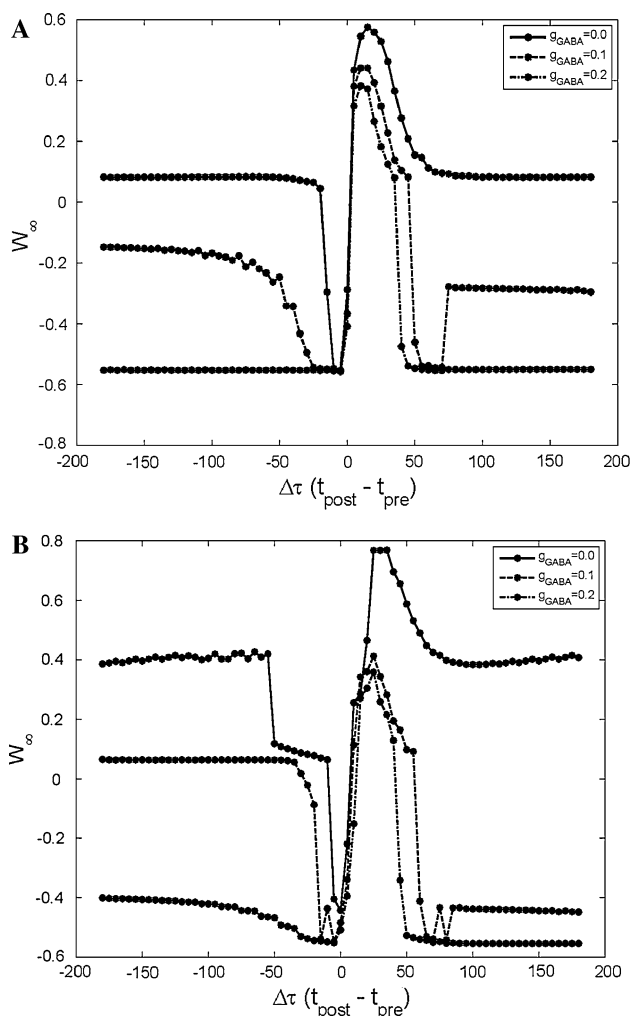


**Fig. 8** Saturated synaptic weight ( $W_{\infty}$ ) values as a function of interstimulus time interval,  $\Delta\tau = t_{\text{postSpike}} - t_{\text{preBurst}}$ .  $\Delta\tau$  ranges from  $-180$  to  $180$  ms in increments of  $5$  ms. An  $100$  Hz GABA spike train is present within  $\Delta\tau$ . **a** Burst ISI is set to  $5$  ms. **b** Burst ISI is set to  $10$  ms

NMDAR channels. Similar effects occur through the VGCC.

Pairing of a SR burst and a somatic burst in the absence of inhibition (see Fig. 14a, b)

When a dendritic burst is paired with a somatic burst the symmetry-to-asymmetry transition is evident even in the absence of inhibition. This transition appears to be a function of bISI, where the STDP curve shifts to an asymmetrical shaped curve with the peak LTP and LTD values are  $+5$  and  $-10$  ms, respectively as bISI increases (see Fig. 15).

In the paired preBurst-30-postBurst stimulation protocol (see Fig. 16a), where a presynaptic (dendritic) burst stimulation is followed  $30$  ms later by a postsynaptic (somatic) burst stimulation, a low peaked calcium influx through the

NMDA channels is evident in the dendrite followed by a second high peaked calcium influx through the VGCC. In the case where bISI is  $5$  ms the second calcium spike is doubled and remained above the  $4 \mu\text{M}$  threshold for longer period of time than when bISI is  $2$  ms. Thus, the level of potentiation (P) when bISI is  $5$  ms is higher than when bISI is  $2$  ms (see Fig. 15). In the preBurst-50-postBurst scenario,  $50$  ms after the presynaptic (dendritic) stimulation a BPAP will arrive at the dendrite causing removal of the magnesium block from the NMDA channels. By then though more and more NMDA channels will be inactivated and hence the calcium influx will be greatly reduced (compare peak calcium level in Fig. 16a, b). The peak calcium level will continue to decrease as the pre-post interstimulus interval is lengthened.

In the postBurst-10-preBurst scenario (see Fig. 16c), the calcium influx is once again greatly reduced due to a different time course than in the preBurst-30-postBurst case. This time most of the calcium comes through the VGCCs producing a slight amplitude increase in calcium influx almost immediately, followed by a second calcium with a lower peak. The valley that separates the two peaks is above the  $0.6 \mu\text{M}$  threshold, but below the  $2 \mu\text{M}$  threshold, which triggers the depression (D) detector, but not the veto (V) detector and produces LTD. In the postBurst-50-preBurst case, the two calcium level peaks are more distinguishable, because of the  $50$  ms delay between the post stimulation and the pre-stimulation (see Fig. 16d). The valley that separates them drops below the  $0.6 \mu\text{M}$  threshold causing a much smaller LTD.

Pairing of a dendritic burst and a somatic burst in the presence of an  $100$  Hz inhibitory spike train as a function of GABA conductance and burst interspike interval (see Fig. 14a, c)

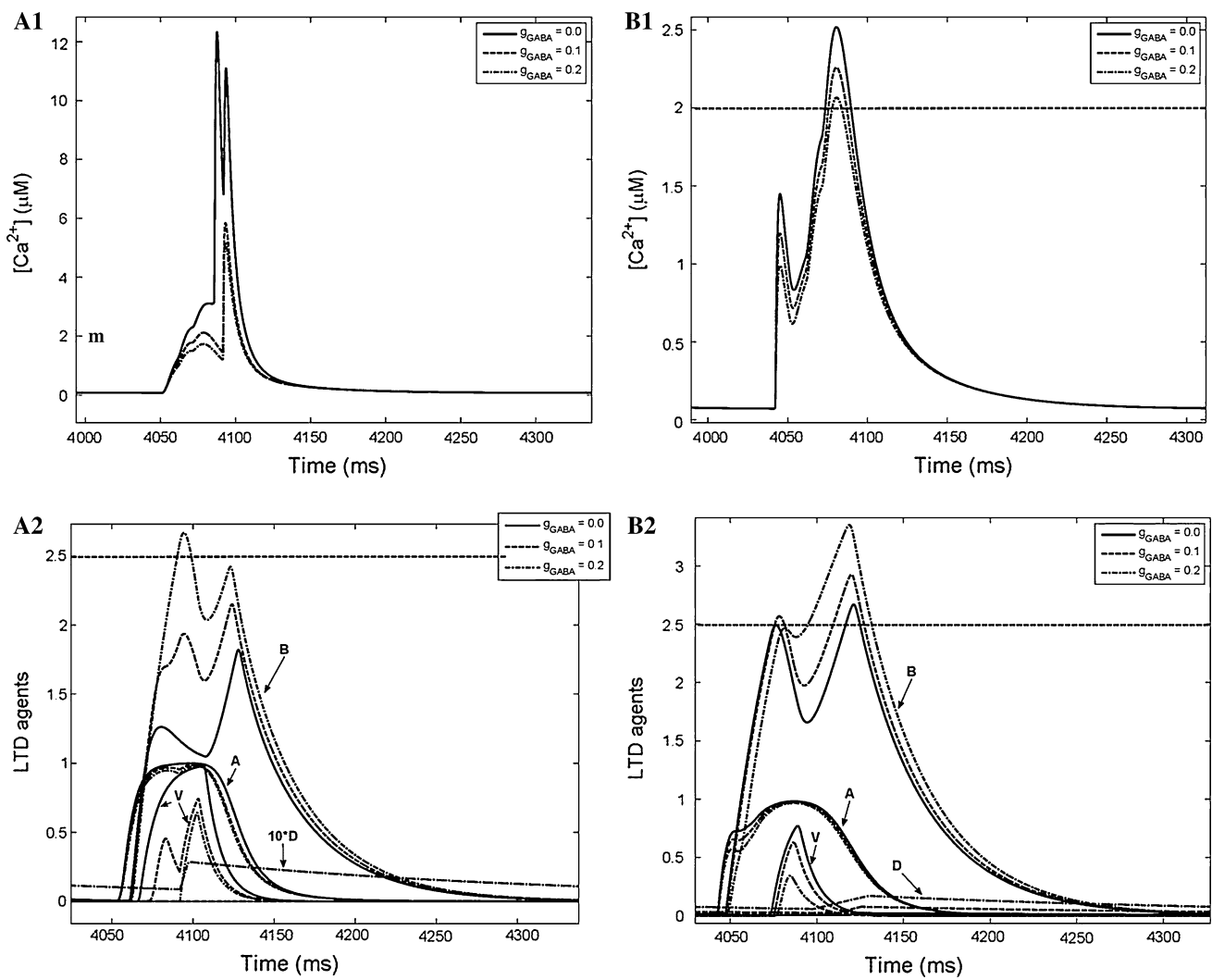
In the presence of inhibition and as a function of bISI the STDP curve transitions from asymmetry when bISI is  $5$  ms to a Mexican-hat symmetry as  $g_{\text{GABA}}$  increases (see Fig. 17b). When bISI is  $2$  ms and when inhibition is absent, the STDP curve is symmetrical with flat tails but shifts to a Mexican-hat symmetry as  $g_{\text{GABA}}$  increases (see Fig. 17a). The peak LTP in both cases is reduced as  $g_{\text{GABA}}$  is increased, but the reduction is stronger when bISI is  $2$  ms.

## Discussion

What have we learned from the model?

A two compartment model of the CA1 pyramidal cell was presented to investigate how spike timing dependent plasticity is induced by natural firing patterns such as bursts,

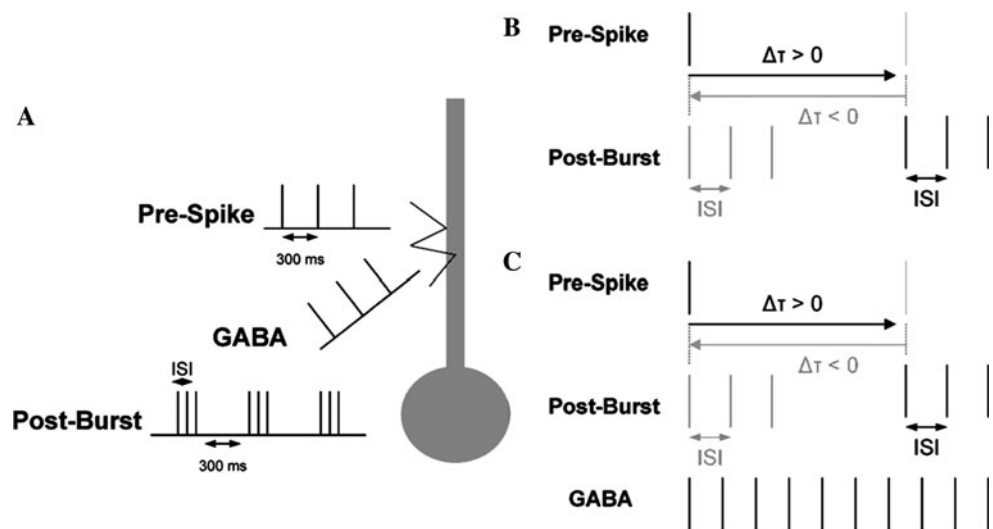




**Fig. 9** Postsynaptic calcium and LTD agents time courses when a presynaptic burst with burst ISI equal to 10 ms is paired with a postsynaptic spike in the presence of an 100 Hz GABA inhibition as a

function of  $g_{GABA}$ . Times shown are measured relative to the onset of the stimulation experiments. (A1 and A2)  $\Delta\tau = +40$  ms. (B1 and B2)  $\Delta\tau = -10$  ms

**Fig. 10 a** Our model CA1 neuron with its three transient inputs to the soma and dendrite. Inputs: an excitatory burst to the dendrite, an excitatory spike to the soma and an inhibitory spike to the dendrite. Each input repeats every 300 ms for about 5 s. **b** Pairing of a dendritic spike with a somatic burst in the absence of inhibition. **c** Pairing of a dendritic spike with a somatic burst in the presence of GABA inhibition



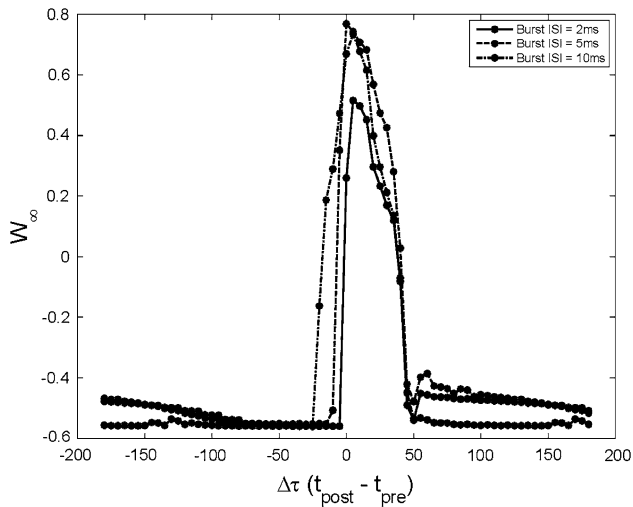


**Fig. 11** Simulated STDP profile as a function of burst interspike interval (burst ISI) in the absence of inhibition.  $\Delta\tau$  ( $t_{\text{postBurst}} - t_{\text{preSpike}}$ ) is the interstimulus interval between the first spike of the somatic burst and the dendritic spike.  $\Delta\tau$  ranges from  $-180$  to  $180$  ms in increments of  $5$  ms. The pairing repeats every  $300$  ms for about  $5$  s

how this plasticity is affected when inhibition is present and how is the STDP curve shaped when theta modulated single spikes, bursts and inhibition interact in the dendrite of the CA1 pyramidal cell. The pyramidal cell model was an extension of the Cutsuridis model (2011) to more complex inputs (bursts), which investigated the conditions under which the STDP curve transitions from asymmetry to symmetry in the presence of inhibition (Aihara et al. 2007; Nishiyama et al. 2000; Tsukada et al. 2005). The present model's dynamics matched the experimental observed canonical form of STDP (Bi and Poo 1998). With the parameter set unchanged it computationally investigated how bursts and inhibition interact to shape the STDP curve. The present model made a number of theoretical predictions:

- The asymmetry of the STDP is a *fixed* property when a dendritic burst with various burst interspike intervals is paired with a somatic spike.
- The symmetry of the STDP is a *fixed* property when a somatic burst with various bISIs is paired with a dendritic spike.
- A *1.6-fold increase* in LTP is evident when  $\Delta\tau = 0-5$  ms as a function of bISI when a somatic burst is paired with a dendritic spike.
- The transition from asymmetry to symmetry can occur *even* in the absence of inhibition when a somatic burst and a dendritic burst are paired together.
- The strength of inhibition ( $g_{\text{GABA}}$ ) is *still* an important factor determining the asymmetry-to-symmetry transition of STDP in all stimulation pairings.

- Inhibition and burst interspike interval are two factors which lead to “global” LTP and/or LTD at large interstimulus intervals  $\Delta\tau$ .

These theoretical predictions can easily be verified by experiments and which may lead to a better understanding of spike timing dependent plasticity in the CA1 pyramidal cell of the hippocampus.

#### Comparison with other models

Although few modeling studies have been published over the years where they attempted to investigate how bursts affect spike timing dependent plasticity, no modeling studies have been published with the exception of the author (Cutsuridis 2011) who tried to study how excitation and inhibition interact to shape the STDP curve. Clopath et al. (2010) introduced a phenomenological model of STPD in which synaptic changes depended on the presynaptic spike arrival and the postsynaptic membrane potential filtered with two different time constants to simulate the development of localized receptive fields in a recurrent network of spiking neurons. Their model used different stimulation protocols consisting of pairs of single spikes and single spikes with bursts and it was successful at describing several of the nonlinear effects observed in STDP experiments in the absence of inhibition. Froemke et al. (2006) considered three models of STDP for predicting synaptic modifications induced by complex spike trains such as bursts. They found that although STDP depends on the burst frequency, later spikes in the burst have a small effect on synaptic modification. Cutsuridis (2011) is the only study and the basis of my present study where the effects of inhibition on spike timing dependent synaptic plasticity were investigated quantitatively. Experimental evidence has shown that the form of STDP is location dependent. More proximal to the soma of a CA1 pyramidal cell the form of STDP is symmetric, whereas more distal to the soma is asymmetric. Cutsuridis (2011) showed that this transition is due to inhibition under certain conditions such as its frequency, strength and relative onset with pre-post excitatory stimulation.

#### Future work

Several extensions to the basic idea of how inhibition affects the STDP profile resulting from the interaction of a burst with a spike or a burst with a burst deserve consideration. A more detailed compartmental model of the CA1 pyramidal neuron has been constructed to model these conditions in the pyramidal cell dendrites (Poirazzi et al. 2003). Experimental evidence has shown that CA1 pyramidal cells receive inputs from the entorhinal cortex to their distal dendrites and from the CA3 Schaffer collaterals

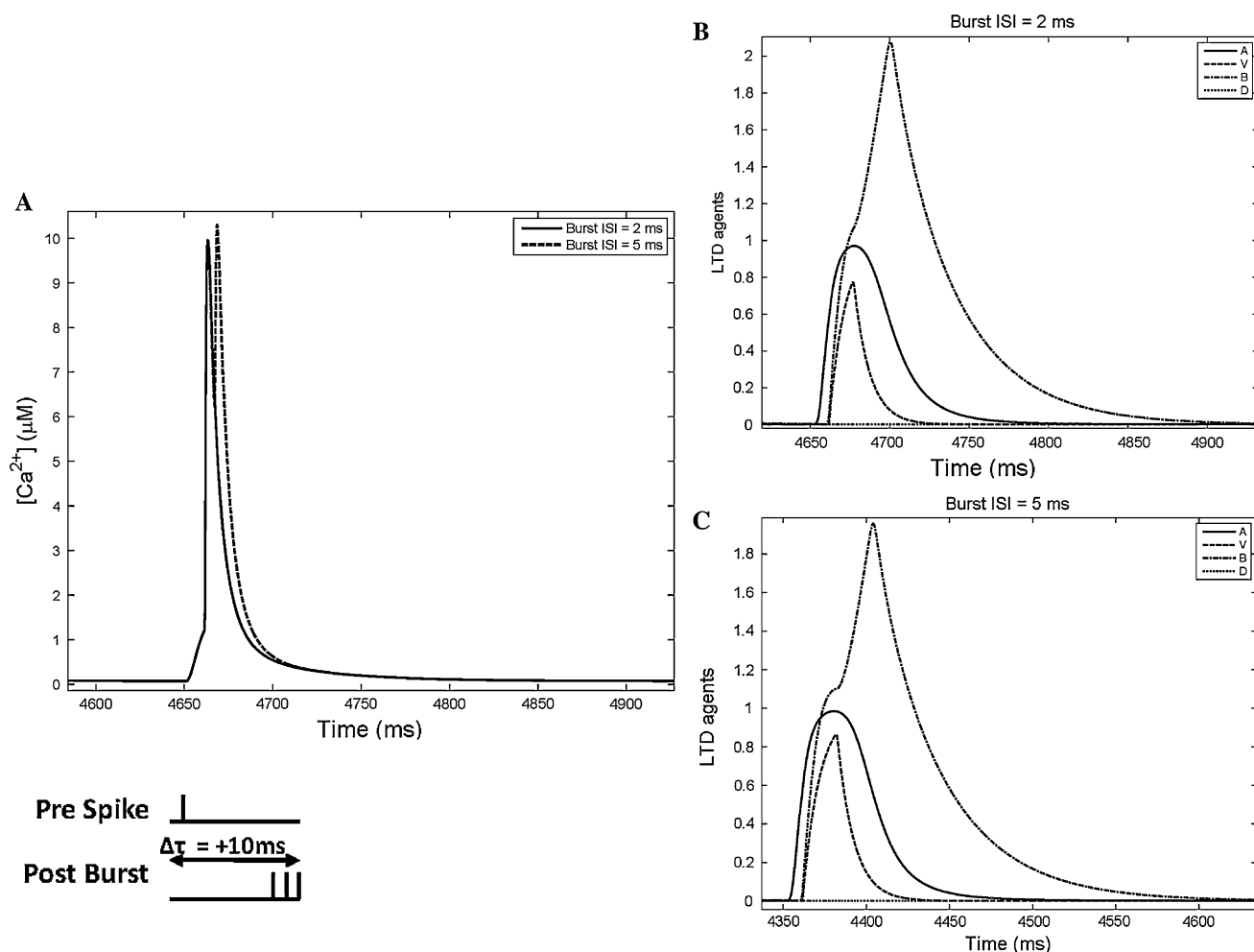


**Fig. 12** (a bottom) Graphical representation of preSpike-(+10 ms)-postBurst stimulation paradigm in the absence of GABA inhibition. (A top) Time course of  $Ca^{2+}$  concentration ( $\mu M$ ) as a function of burst interspike intervals (ISIs) (2 and 5 ms) in the absence of GABA inhibition in the preSpike-(+10 ms)-postBurst scenario. (Middle) Comparative bar graph of potentiation ( $P$ ) and depression ( $D$ ) values

to their proximal ones. Fibers that impinge on pyramidal cell's proximal dendrites immediately above the pyramidal cell bodies form compact synaptic fields, while those impinging on the distal ones form much broader and asymmetrical distributed fields (Shimono et al. 2002). In the absence of the Schaffer collateral inputs, backpropagating action potentials rarely reach the pyramidal cell distal dendrites. The Schaffer collateral input thus provides a boosting mechanism of the bpAP. Work is underway in my laboratory to explore how STDP is dynamically regulated by the interaction between multiple presynaptic inputs impinging on different dendritic compartments of CA1 pyramidal cell (Golding et al. 2002; Letzkus et al. 2006).

Furthermore in CA1, the distal and proximal dendrites of pyramidal neurons are both targeted by the DAergic neurons (Cobb and Lawrence 2010). Previous studies have

for two burst ISIs: 2 and 5 ms. **b** Time course of LTD agents (A, B, V, and D) in the absence of inhibition in the preSpike-(+10 ms)-postBurst scenario when burst ISI is 2 ms. **c** Time course of LTD agents (A, B, V, and D) in the absence of inhibition in the preSpike-(+10 ms)-postBurst scenario when burst ISI is 5 ms

shown that when DA is applied to the bathing solution, the field-EPSP (fEPSP) evoked by the EC temporoammonic (TA) pathway stimulation is depressed, whereas the fEPSP by the CA3 Schaffer collateral (SC) pathway stimulation remains unaltered (Otmakhova and Lisman 1999). Subsequent studies by Ito and Schuman (2007) demonstrated that DA acts as a gate on the direct cortical input to the CA1 PC distal dendrites, modulating the information flow and the synaptic plasticity in a frequency-dependent manner. During low frequency stimulation, DA depresses the excitatory TA inputs to both CA1 pyramidal cells and NGL interneurons via presynaptic inhibition, whereas during high frequency stimulation, DA potently facilitates the TA excitatory drive onto CA1 pyramidal neurons, while diminishing the feedforward NGL inhibition to the distal PC dendrites. Understanding the cellular mechanisms by which dopamine modulation interacts with spike timing

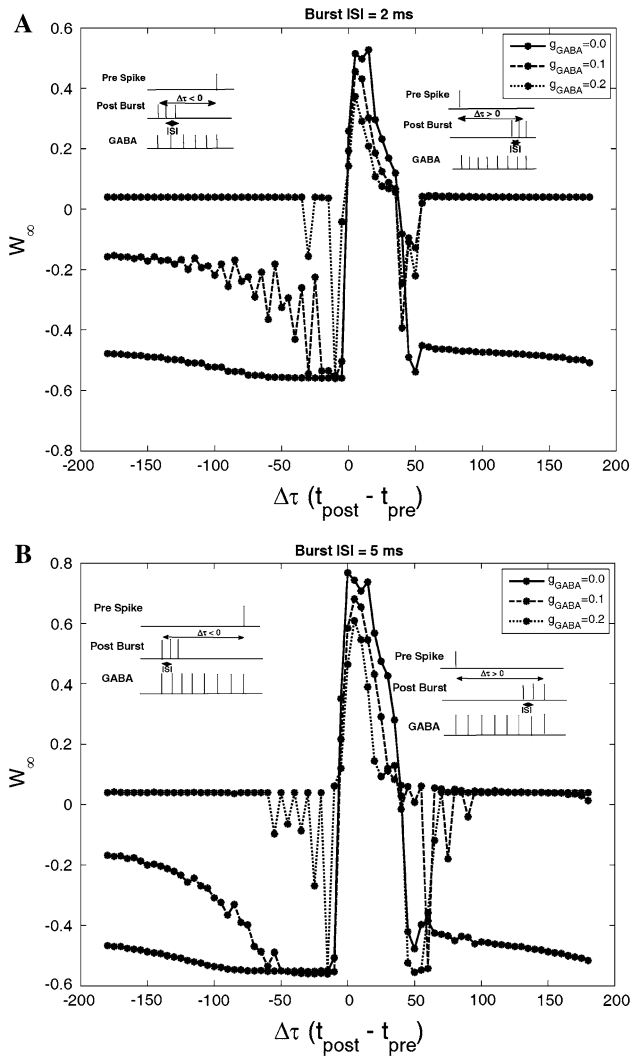


**Fig. 13** Saturated synaptic weight ( $W_\infty$ ) values as a function of interstimulus time interval,  $\Delta\tau = t_{\text{postBurst}} - t_{\text{preSpike}}$ , between a dendritic (pre) spike and a somatic (post) burst.  $\Delta\tau$  ranges from  $-180$  to  $180$  ms in increments of  $5$  ms. An  $100$  Hz GABA spike train is present within  $\Delta\tau$ . **a** Burst ISI is set to  $2$  ms. **b** Burst ISI is set to  $5$  ms

dependent plasticity is an important step in understanding how STDP works in more realistic settings.

**Acknowledgments** This work was supported by the EPSRC project grant EP/D04281X/1 and the NSF Science of Learning Center CELEST grant SMA-0835976.

**Conflict of interests** The author has declared that no competing interests exist.

## Appendix

The somatic ( $s$ ) and dendritic ( $d$ ) compartments of the pyramidal neuron obey the following current balance equations

$$C_m \frac{dV_s}{dt} = I_L + I_{Na,s} + I_{K_{dr,s}} + I_{A,s} + I_{m,AHAP,s} + I_{CaL,s} + I_{coup} + I_{in} \cdot F_{post} \quad (4)$$

$$C_m \frac{dV_d}{dt} = I_L + I_{Na,d} + I_{K_{dr,d}} + I_{A,d} + I_{m,AHAP,d} + I_{CaL,d} + I_{coup} + I_{AMPA} + I_{NMDA} + I_{GABA} \quad (5)$$

where  $I_L$  is the leak current,  $I_{Na}$  is the sodium current,  $I_{K_{dr}}$  is the delayed rectifier potassium current,  $I_A$  is the type A potassium current,  $I_{m,AHP}$  is the medium  $Ca^{2+}$  activated  $K^+$  after-hyper-polarization current,  $I_{CaL}$  is the L-type  $Ca^{2+}$  current,  $I_{coup}$  is the electrical coupling between compartments,  $I_{in}$  is the injected current,  $I_{AMPA}$  is the AMPA current,  $I_{NMDA}$  is the NMDA current and  $I_{GABA}$  is the GABA current.

The sodium current at the soma is described by:

$$I_{Na,s} = -g_{Na,s} \cdot M_{Na,s}^2 \cdot H_{Na,s} \cdot (V_s - V_{Na}) \quad (6)$$

where  $g_{Na,s}$  is the maximal conductance of the  $Na^+$  current,  $M_{Na,s}$  and  $H_{Na,s}$  are the activation and inactivation constants and  $V_{Na}$  is the reversal potential of the  $Na^+$  current. The activation and inactivation constants at the soma are given by

$$M_{Na,s} = \alpha_{M,s}(V_s) / (\alpha_{M,s}(V_s) + \beta_{M,s}(V_s))$$

$$\alpha_{M,s}(V_s) = 0.32 \cdot (-46.9 - V_s) / (\exp((-46.9 - V_s)/4.0) - 1.0)$$

$$\beta_{M,s}(V_s) = 0.28 \cdot (V_s + 19.9) / (\exp((V_s + 19.9)/5.0) - 1.0)$$

$$H'_{Na,s} = \alpha_{H,s}(V_s) - (\alpha_{H,s}(V_s) + \beta_{H,s}(V_s)) \cdot H_{Na,s}$$

$$\alpha_{H,s}(V_s) = 0.128 \cdot \exp((-43 - V_s)/18)$$

$$\beta_{H,s}(V_s) = 4 / (1 + \exp((-20 - V_s)/5))$$

The sodium current at the dendrite is described by:

$$I_{Na,d} = -g_{Na,d} \cdot M_{Na,d}^2 \cdot H_{Na,d} \cdot D_{Na,d} \cdot (V_d - V_{Na}) \quad (7)$$

where

$$M'_{Na,d} = (M_{\infty Na,d} - M_{Na,d}) / \tau_{M_{Na,d}}$$

$$M_{\infty Na,d} = 1 / (1 + \exp((-V_d - 40)/3))$$

$$\tau_{M_{Na,d}} = \max(0.1, 0.05)$$

$$H'_{Na,d} = (H_{\infty Na,d} - H_{Na,d}) / \tau_{H_{Na,d}}$$

$$H_{\infty Na,d} = 1 / (1 + \exp((V_d + 45)/3))$$

$$\tau_{H_{Na,d}} = 0.5$$

$$D'_{Na,d} = (D_{\infty Na,d} - D_{Na,d}) / \tau_{D_{Na,d}}$$

$$D_{\infty Na,d} = (1 + n_{att} \cdot \exp((V_d + 60)/2)) / (1 + \exp((V_d + 60)/2))$$

**Fig. 14** **a** Our model CA1 neuron with its three transient inputs to the soma and dendrite. Inputs: an excitatory burst to the dendrite, an excitatory burst to the soma and an inhibitory spike to the dendrite. Each input repeats every 300 ms for about 5 s. **b** Pairing of a dendritic burst with a somatic burst in the absence of inhibition. **c** Pairing of a dendritic burst with a somatic burst in the presence of GABA inhibition

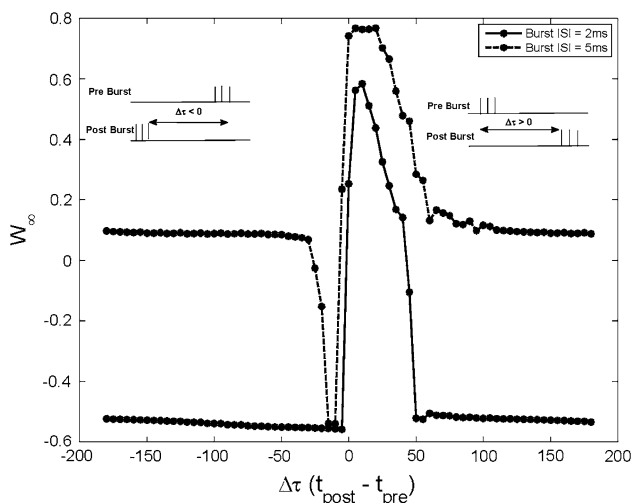
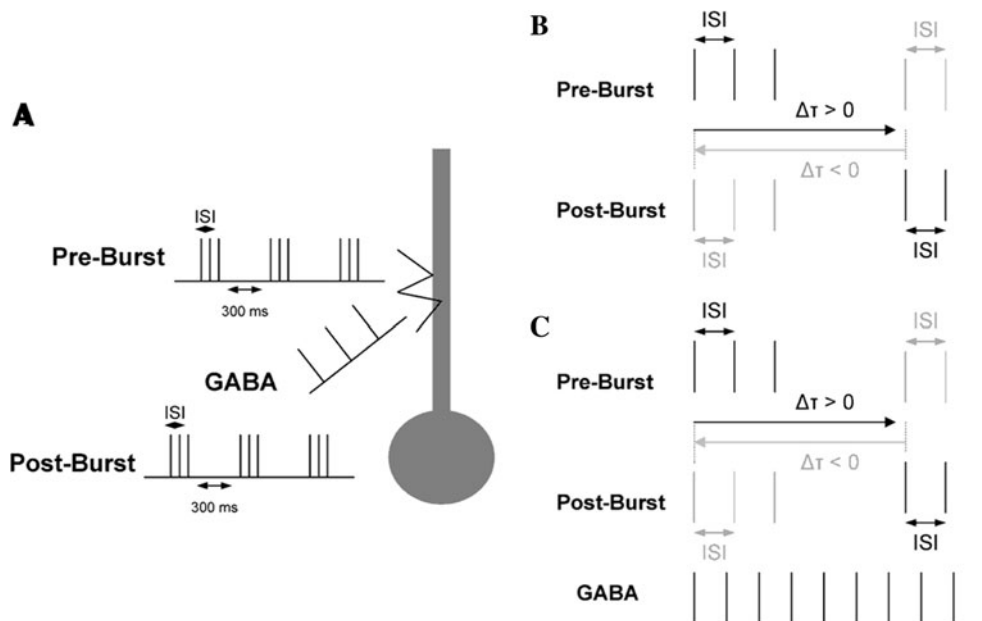


**Fig. 15** Simulated STDP profile as a function of burst interspike interval (burst ISI) in the absence of inhibition.  $\Delta\tau$  ( $t_{\text{postBurst}} - t_{\text{preBurst}}$ ) is the interstimulus interval between the first spike of the dendritic (pre) burst and the first spike of the somatic (post) burst.  $\Delta\tau$  ranges from  $-180$  to  $180$  ms in increments of  $5$  ms. The pairing repeats every  $300$  ms for about  $5$  s

$$\tau_{D_{Na,d}} = \max(0.1, (0.00333 \cdot \exp(0.0024 \cdot (V_d + 60) \cdot Q)) / (1 + \exp(0.0012 \cdot (V_d + 60) \cdot Q)))$$

$$Q = 96480 / (8.315 \cdot (273.16 + T))$$

where  $T$  is the temperature in Celcius and  $natt$  is the  $\text{Na}^+$  attenuation.

The type-A  $\text{K}^+$  current at the soma is given by

$$I_{K_{A,s}} = -g_{K_{A,s}} \cdot A_s \cdot B_s \cdot (V_s - V_K) \quad (8)$$

where  $g_{K_{A,s}}$  is the maximal conductance,  $V_k$  is the reversal potential,  $A_s$  and  $B_s$  are the activation and inactivation

constants. The activation and inactivation constants are given by

$$A'_s = (A_{\infty_s} - A_s) / \tau_{A_s}$$

$$A_{\infty_s} = 1 / (1 + A_{\alpha,s})$$

$$A_{\alpha,s} = \exp(0.001 \cdot \zeta(V_s) \cdot (V_s - 11) \cdot Q)$$

$$\tau_{A_s} = \max(A_{\beta,s} / ((1 + A_{\alpha,s}) \cdot QT \cdot 0.05), 0.1)$$

$$A_{\beta,s} = \exp(0.00055 \cdot Q \cdot (V_s - 11) \cdot \zeta(V_s))$$

$$\zeta(V_s) = -1.5 - (1 / (1 + \exp((V_s + \zeta_p) / 5)))$$

$$QT = 5^{((T-24) / 10)}$$

$$B'_s = (B_{\infty_s} - B_s) / \tau_{B_s}$$

$$B_{\infty_s} = 0.3 + 0.7 / (1 + \exp(0.02 \cdot (V_s + 63.5) \cdot Q))$$

$$\tau_{B_s} = \kappa \cdot \max(0.11 \cdot (V_s + 62), 2)$$

The type-A  $\text{K}^+$  current at the dendrite is given by

$$I_{K_{A,d}} = -g_{K_{A,d}} \cdot A_d \cdot B_d \cdot (V_d - V_K) \quad (9)$$

The activation and inactivation constants are given by

$$A'_d = (A_{\infty_d} - A_d) / \tau_{A_d}$$

$$A_{\infty_d} = 1 / (1 + A_{\alpha,d})$$

$$A_{\alpha,d} = \exp(asap \cdot \zeta(V_d) \cdot (V_d + 1) \cdot Q)$$

$$A_{\beta,d} = \exp(0.00039 \cdot Q \cdot (V_d + 1) \cdot \zeta_2(V_d))$$

$$\tau_{A_d} = \max(A_{\beta,d} / ((1 + A_{\alpha,d}) \cdot QT \cdot 0.1), 0.1)$$

$$\zeta(V_d) = -1.5 - (1 / (1 + \exp((V_d + \zeta_p) / 5)))$$

$$\zeta_2(V_d) = -1.8 - (1 / (1 + \exp((V_d + 40) / 5)))$$



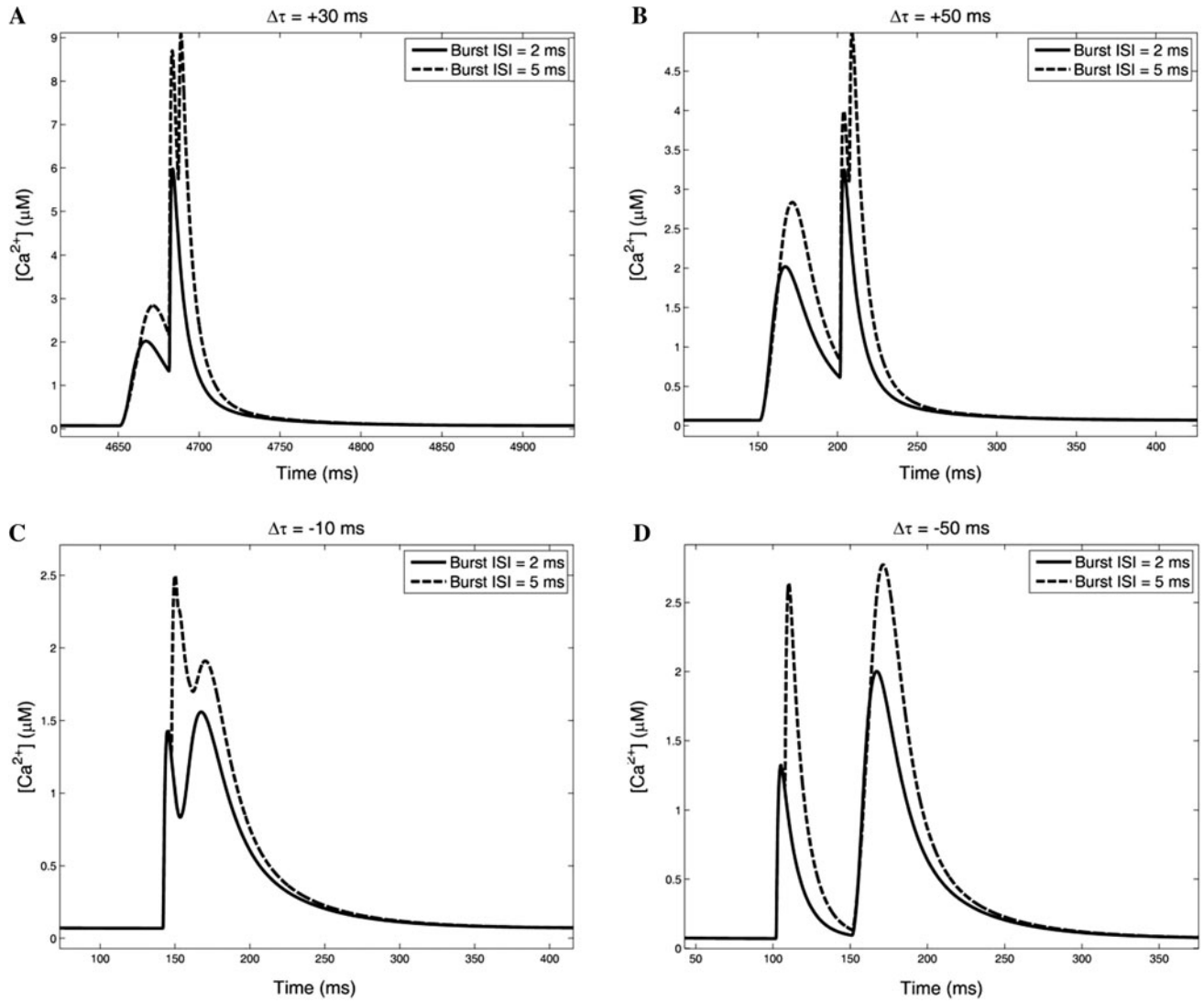


**Fig. 16** Postsynaptic calcium time courses in the absence of inhibition. Times shown are measured relative to the onset of the stimulation experiments. **a** preBurst-(+30)-postBurst case. **b** preBurst-(+50)-

postBurst case. **c** postBurst(-10)-preBurst case. **d** postBurst(-50)-preBurst case

$$B'_d = (B_{\infty d} - B_d) / \tau_{B_d}$$

$$B_{\infty d} = 0.3 + 0.7 / (1 + \exp(\text{inact}_2 \cdot (V_s + \text{inact}) \cdot Q))$$

$$\tau_{B_d} = \kappa \cdot \max(\text{inact}_3 \cdot (V_s + \text{inact}_4), \text{inact}_5)$$

The delayed rectifier  $K^+$  current at the soma is given by

$$I_{K_{dr,s}} = -g_{K_{dr,s}} \cdot N_s \cdot (V_s - V_K) \quad (10)$$

where  $g_{K_{dr,s}}$  is the maximal conductance. The activation constant,  $N_s$  is given by

$$N'_s = \alpha_{N_s}(V_s) - (\alpha_{N_s}(V_s) + \beta_{N_s}(V_s)) \cdot N_s$$

$$\alpha_{N_s}(V_s) = 0.016 \cdot (-24.9 - V_s) / (\exp((-24.9 - V_s) / 5) - 1)$$

$$\beta_{N_s}(V_s) = 0.25 \cdot \exp(-1 - 0.025 \cdot V_s)$$

The delayed rectifier  $K^+$  current at the dendrite is given by

$$I_{K_{dr,d}} = -g_{K_{dr,d}} \cdot N_d^2 \cdot (V_d - V_K) \quad (11)$$

where  $g_{K_{dr,d}}$  is the maximal conductance. The activation constant,  $N_d$  is given by

$$N'_d = (N_{\infty d} - N_d) / \tau_{N_d}$$

$$N_{\infty d} = 1 / (1 + \exp((-V_d - 42) / 2))$$

$$\tau_{N_d} = 2.2$$

The medium  $Ca^{2+}$  activated  $K^+$  after hyperpolarization current is given by

$$I_{mAHP} = -g_{mAHP} \cdot Q_m \cdot (V_s - V_K) \quad (12)$$

where  $g_{K_{mAHP}}$  is the maximal conductance. The activation constant,  $Q_m$  is given by

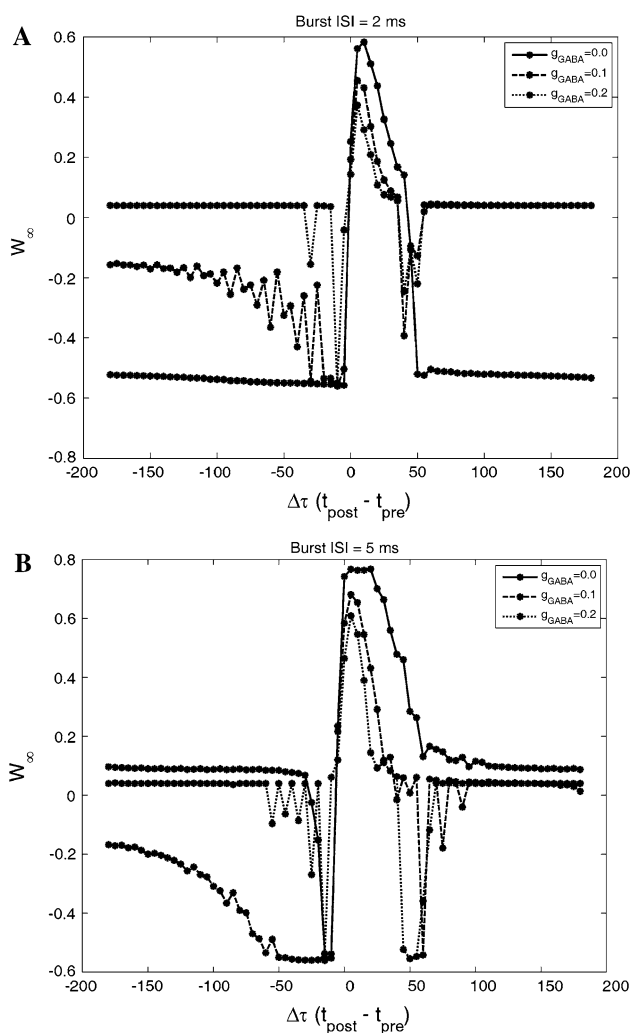


**Fig. 17** Saturated synaptic weight ( $W_\infty$ ) values as a function of interstimulus time interval,  $\Delta\tau = t_{\text{postBurst}} - t_{\text{preBurst}}$ , between a dendritic (pre) burst and a somatic (post) burst.  $\Delta\tau$  ranges from  $-180$  to  $180$  ms in increments of  $5$  ms. An  $100$  Hz GABA spike train is present within  $\Delta\tau$ . **a** Burst ISI is set to  $2$  ms. **b** Burst ISI is set to  $5$  ms

$$Q'_m = (Q_{m_\infty} - Q_m) / \tau_{Q_m}$$

$$Q_{m_\infty} = q_{\text{hat}} \cdot Q_{m_x} \cdot \tau_{Q_m}$$

$$Q_{m_x} = q_{\text{ma}} \cdot \chi / (0.001 \cdot \chi + 0.18 \cdot \exp(-1.68 \cdot V_s \cdot Q))$$

$$Q_{m_\beta} = (q_{\text{mb}} \cdot \exp(-0.022 \cdot V_s \cdot Q)) / (\exp(-0.022 \cdot V_s \cdot Q) + 0.001 \cdot \chi)$$

$$\tau_{Q_m} = 1 / (Q_{m_x} + Q_{m_\beta})$$

The L-type  $\text{Ca}^{2+}$  current at the soma is described by

$$I_{\text{CaL}_s} = -g_{\text{CaL}_s} \cdot S_s \cdot g_{\text{hk}}(V_s, \chi_s) \cdot (1 / (1 + \chi_s)) \quad (13)$$

where  $g_{\text{CaL}_s}$  is the maximal conductance and

$$S'_s = (S_{\infty_s} - S_s) / \tau_{S_s}$$

$$S_{\infty_s} = \alpha_s(V_s) / (\alpha_s(V_s) + \beta_s(V_s))$$

$$\tau_{S_s} = 1 / (5 \cdot (\alpha_s(V_s) + \beta_s(V_s)))$$

$$\alpha_s(V_s) = -0.055 \cdot (V_s + 27.01) / (\exp((-V_s - 27.01) / 3.8) - 1)$$

$$\beta_s(V_s) = 0.94 \cdot \exp((-V_s - 63.01) / 17)$$

$$xx = 0.0853 \cdot (273.16 + T) / 2$$

$$f(z) = (1 - z/2) \cdot f_2(z) + (z / (\exp(z) - 1)) \cdot f_3(z)$$

$$f_2(z) = H(0.0001 - |z|)$$

$$f_3(z) = H(|z| - 0.0001)$$

$$g_{\text{hk}} = -xx \cdot (1 - ((\chi_s / \text{Ca}) \cdot \exp(V_s / xx))) \cdot f(V_s / xx)$$

$$\chi'_s = \phi_s \cdot I_{\text{CaL}_s} - (\beta_s \cdot (\chi_s - \chi_{0,s})) + (\chi_d - \chi_s) / \text{Ca}\tau - (\beta_s / \text{nonc}) \cdot \chi_s^2$$

$$\chi'_d = \phi_d \cdot (I_{\text{CaL}_d} + I_{\text{Ca,NMDA}}) - \beta_d \cdot (\chi_d - \chi_{0,d}) - (\beta_d / \text{nonc}) \cdot \chi_d^2 - \text{buff} \cdot \chi_d$$

where  $\chi_s$  and  $\chi_d$  are the  $\text{Ca}^{2+}$  concentrations in the soma and dendrite, respectively. The L-type  $\text{Ca}^{2+}$  current at the dendrite is described by

$$I_{\text{CaL}_d} = -g_{\text{CaL}_d} \cdot S'_d \cdot T_d \cdot (V_d - V_{\text{Ca}}) \quad (14)$$

$$S'_d = (S_{\infty_d} - S_d) / \tau_{S_d}$$

$$S_{\infty_d} = 1 / (1 + \exp(-V_d - 37))$$

$$\tau_{S_d} = s_3 + s_1 / (1 + \exp(V_d + s_2))$$

$$T'_d = (T_{\infty_d} - T_d) / \tau_{T_d}$$

$$T_{\infty_d} = 1 / (1 + \exp((V_d + 41) / 0.5))$$

$$\tau_{T_d} = 29$$

The coupling constant for the compartment  $i$  is

$$I_{\text{coup}} = g_{\text{coup}} \cdot (V_j - V_i) \quad (15)$$

The  $\text{Ca}^{2+}$ -NMDA, AMPA, GABA-A and NMDA synaptic currents are given by

$$I_{\text{Ca,NMDA}} = -g_{\text{Ca,NMDA}} \cdot s_{\text{NMDA}} \cdot m_{\text{Ca,NMDA}} \cdot (V_d - V_{\text{Ca,NMDA}}) \quad (16)$$

$$I_{\text{NMDA}} = -g_{\text{NMDA}} \cdot s_{\text{NMDA}} \cdot m_{\text{NMDA}} \cdot (V_d - V_{\text{NMDA}}) \quad (17)$$

$$I_{\text{AMPA}} = -g_{\text{AMPA}} \cdot s_{\text{AMPA}} \cdot (V_d - V_{\text{AMPA}}) \quad (18)$$

$$I_{\text{GABA}} = -g_{\text{GABA}} \cdot s_{\text{GABA}} \cdot (V_d - V_{\text{GABA}}) \quad (19)$$

where

$$m_{\text{NMDA}} = 1 / (1 + 0.3 \cdot \text{Mg} \cdot \exp(-0.062 \cdot V_d))$$

$$m_{\text{Ca,NMDA}} = 1 / (1 + 0.3 \cdot \text{Mg} \cdot \exp(-0.124 \cdot V_d))$$

with  $\text{Mg}^{2+} = 2$  mM. The activation equations for AMPA, NMDA and GABA-A currents are

$$s_x = s_{x_{\text{fast}}} + s_{x_{\text{slow}}} + s_{x_{\text{rise}}} \quad (20)$$

where  $x$  stands for AMPA, NMDA, GABA and

$$s'_{NMDA_{rise}} = -20 \cdot (1 - s_{NMDA_{fast}} - s_{NMDA_{slow}}) \cdot F_{pre} - (1/NMDA_{rate}) \cdot s_{NMDA_{rise}}$$

$$s'_{NMDA_{fast}} = 20 \cdot (0.527 - s_{NMDA_{fast}}) \cdot F_{pre} - (1/ndf) \cdot s_{NMDA_{fast}}$$

$$s'_{NMDA_{slow}} = 20 \cdot (0.473 - s_{NMDA_{slow}}) \cdot F_{pre} - (1/nds) \cdot s_{NMDA_{slow}}$$

$$s'_{AMPA_{rise}} = -20 \cdot (1 - s_{AMPA_{fast}} - s_{AMPA_{slow}}) \cdot F_{pre} - (1/0.58) \cdot s_{AMPA_{rise}}$$

$$s'_{AMPA_{fast}} = 20 \cdot (0.903 - s_{AMPA_{fast}}) \cdot F_{pre} - (1/7.6) \cdot s_{AMPA_{fast}}$$

$$s'_{AMPA_{slow}} = 20 \cdot (0.097 - s_{AMPA_{slow}}) \cdot F_{pre} - (1/25.69) \cdot s_{AMPA_{slow}}$$

and

$$s'_{GABA_{rise}} = -20 \cdot (1 - s_{GABA_{fast}} - s_{GABA_{slow}}) \cdot F_{GABA} - (1/1.18) \cdot s_{GABA_{rise}}$$

$$s'_{GABA_{fast}} = 20 \cdot (0.803 - s_{GABA_{fast}}) \cdot F_{GABA} - (1/8.5) \cdot s_{GABA_{fast}}$$

$$s'_{GABA_{slow}} = 20 \cdot (0.197 - s_{GABA_{slow}}) \cdot F_{GABA} - (1/30.01) \cdot s_{GABA_{slow}}$$

The calcium detector model is governed by the following six equations:

$$P' = (\phi_a(\chi_d) - c_p \cdot A \cdot P) / \tau_p \tag{21}$$

$$V' = (\phi_b(\chi_d) - V) / \tau_V \tag{22}$$

$$A' = (\phi_c(\chi_d) - A) / \tau_A \tag{23}$$

$$B' = (\phi_e(A) - B - c_d \cdot B \cdot V) / \tau_B \tag{24}$$

$$D' = (\phi_d(B) - D) / \tau_D \tag{25}$$

$$W' = (\alpha_w / (1 + \exp((P - a) / p_a)) - \beta_w / (1 + \exp((D - d) / p_d)) - W) / \tau_w \tag{26}$$

where  $P$  is the potentiation detector dynamics,  $V$  is the veto detector dynamics,  $D$  is the depression detector dynamics,  $A$  and  $B$  are the intermediate steps leading up to  $D$  and  $W$  is the readout variable (see Fig. 1). The Hill equations are

$$\phi_a(x) = num_a \cdot ((x/CmHC)^{CmHN}) / (1 + (x/CmHC)^{CmHN}) \tag{27}$$

$$\phi_b(x) = num_b \cdot ((x/CnHC)^{CnHN}) / (1 + (x/CnHC)^{CnHN}) \tag{28}$$

$$\phi_c(x) = num_c / (1 + \exp((x - \theta_c) / \sigma_c)) \tag{29}$$

$$\phi_d(x) = num_d / (1 + \exp((x - \theta_d) / \sigma_d)) \tag{30}$$

## References

- Abarbanel HDI, Gibb L, Huerta R, Rabinovich MI (2003) Biophysical model of synaptic plasticity dynamics. *Biol Cybern* 89:214–226
- Aihara T, Abiru Y, Yamazaki Y, Watanabe H, Fukushima Y, Tsukada M (2007) The relation between spike-timing dependent plasticity and  $Ca^{2+}$  dynamics in the hippocampal CA1 network. *Neuroscience* 145:80–87
- Allen C, Stevens CF (1994) An evaluation of causes for unreliability of synaptic transmission. *Proc Natl Acad Sci USA* 91(22):10380–10383
- Bell CC, Han VZ, Sugawara Y, Grant K (1997) Synaptic plasticity in a cerebellum-like structure depends on temporal order. *Nature* 387:278–281
- Bender VA, Bender KJ, Brasier DJ, Feldman DE (2006) Two coincidence detectors for spike-timing-dependent plasticity in somatosensory cortex. *J Neurosci* 26:4166–4177
- Bi GQ (2002) Spatiotemporal specificity of synaptic plasticity: cellular rules and mechanisms. *Biol Cybern* 87(5–6):319–332
- Bi GQ, Poo MM (1998) Synaptic modifications in cultured hippocampal neurons: dependence on spike timing, synaptic strength, and postsynaptic cell type. *J Neurosci* 18:10464–10472
- Bi GQ, Rubin J (2005) Timing in synaptic plasticity: from detection to integration. *TINS* 28(5):222–228
- Bienenstock EL, Cooper L, Munro P (1982) Theory for the development of neuron selectivity: orientation specificity and binocular interaction in visual cortex. *J Neurosci* 2(1):32–48
- Bliss TV, Collingridge GL (1993) A synaptic model of memory: long-term potentiation in the hippocampus. *Nature* 361:31–39
- Bliss TV, Lomo T (1970) Plasticity in a monosynaptic cortical pathway. *J Physiol* 207(2):61p
- Caporale N, Dan Y (2009) Spike timing dependent plasticity: a Hebbian learning rule. *Ann Rev Neurosci* 31:25–46
- Cassenaer S, Laurent G (2007) Hebbian STDP in mushroom bodies facilitates the synchronous flow of olfactory information in locusts. *Nature* 448:709–713
- Clopath C, Busing L, Vasilaki E, Gerstner W (2010) Connectivity reflects coding: a model of voltage-based STDP with homeostasis. *Nat Neurosci* 13(3):344–352
- Cobb S, Lawrence JJ (2010) Neuromodulation of hippocampal cells and circuits. In: Cutsuridis V et al (eds) *Hippocampal microcircuits: a computational Modeller's resource book*. Springer, New York, pp 187–246
- Cobb SR, Buhl EH, Halacy K, Paulsen O, Somogyi P (1995) Synchronization of neuronal activity in hippocampus by individual GABAergic interneurons. *Nature* 378:75–77
- Cutsuridis V (2010) Action potential bursts modulate the NMDA-R mediated spike timing dependent plasticity in a biophysical model. In: Diamantaras K, Duch W, Iliadis LS (eds) *ICANN 2010, Part I, LNCS 6352*, Springer, Berlin, pp 107–116
- Cutsuridis V (2011) GABA inhibition modulates NMDA-R mediated spike timing-dependent plasticity (STDP) in a biophysical model. *Neural Netw* 24(1):29–42
- Cutsuridis V, Wennekers T (2009) Hippocampus, microcircuits and associative memory. *Neural Netw* 22(8):1120–1128
- Cutsuridis V, Cobb S, Graham BP (2008) Encoding and retrieval in a CA1 microcircuit model of the hippocampus. In: Kurkova V, Neruda R, Koutnik J (eds) *ICANN 2008, LNCS 5164*. Springer, Berlin, pp 238–247
- Cutsuridis V, Cobb S, Graham BP (2009a) How bursts shape the STDP curve in the presence/absence of GABA inhibition. In: Alippi C et al. (eds) *LNCS 5768*. Springer, Berlin, pp 229–238
- Cutsuridis V, Cobb S, Graham BP (2009b) Modelling the STDP symmetry-to-asymmetry transition in the presence of GABAergic inhibition. *Neural Netw World* 19(5):471–481

- Cutsuridis V, Cobb S, Graham BP (2010a) Encoding and retrieval in the hippocampal CA1 microcircuit model. *Hippocampus* 20(3): 423–446
- Cutsuridis V, Graham BP, Cobb S, Vida I (2010b) Hippocampal microcircuits: a computational modeler's resource book. Springer, New York
- Cutsuridis V, Graham BP, Cobb S, Hasselmo M (2011) Bio-inspired models of recall performance, memory capacity and theta phase precession. In: *IJCNN 2011*, San Jose, CA, July 31–Aug 5
- Debanne D, Gähwiler BH, Thompson SM (1998) Long-term synaptic plasticity between pairs of individual CA3 pyramidal cells in rat hippocampal slice cultures. *J Physiol* 507:237–247
- Ermentrout B (2002) Simulating, analyzing and animating dynamical systems. A guide to XPPAUT for researchers and students. SIAM, Philadelphia
- Feldman DE (2000) Timing-based LTP and LTD at vertical inputs to layer II/III pyramidal cells in rat barrel cortex. *Neuron* 27: 45–56
- Froemke RC, Dan Y (2002) Spike-timing-dependent synaptic modification induced by natural spike trains. *Nature* 416:433–438
- Froemke RC, Poo MM, Dan Y (2005) Spike-timing-dependent synaptic plasticity depends on dendritic location. *Nature* 434(7030): 221–225
- Froemke RC, Tsay IA, Raad M, Long JD, Dan Y (2006) Contribution of individual spikes in burst-induced long term synaptic modification. *J Neurophysiol* 95:1620–1629
- Gloveli T, Kopell N, Dugladze T (2010) Network activity patterns during hippocampal network oscillations in vitro. In: Cutsuridis V et al. (eds) *Hippocampal microcircuits: a computational modeler's resource book*. Springer series in computational neuroscience, vol 5. Springer, Berlin, pp 247–276
- Golding NL, Staff NP, Spruston N (2002) Dendritic spikes as a mechanism for cooperative long-term potentiation. *Nature* 418:326–331
- Hayashi H, Igarashi J (2009) LTD windows of the STDP learning rule and synaptic connections having a large transmission delay enable robust sequence learning amid background noise. *Cogn Neurodyn* 3:119–130
- Hebb DO (1949) *The organization of behavior*. Wiley, New York
- Ismailov I, Kalikulov D, Inoue T, Friedlander MJ (2004) The kinetic profile of intracellular calcium predicts long-term potentiation and long-term depression. *J Neurosci* 24(44):9847–9861
- Ito HT, Schuman EM (2007) Frequency-dependent gating of synaptic transmission and plasticity by dopamine. *Front Neural Circ* 1(1):1–13
- Izhikevich EM, Desai NS, Walcott EC, Hoppensteadt FC (2003) Bursts as a unit of neural information: selective communication via resonance. *TINS* 26(3):161–167
- Jarsky T, Roxin A, Kath WL, Spruston N (2005) Conditional dendritic spike propagation following distal synaptic activation of hippocampal CA1 pyramidal neurons. *Nat Neurosci* 8(12): 1667–1676
- Kampa BM, Stuart GJ (2006) Calcium spikes in basal dendrites of layer 5 pyramidal neurons during action potential bursts. *J Neurosci* 26:7424–7432
- Kampa BM, Clemens J, Jonas P, Stuart GJ (2004) Kinetics of  $Mg^{2+}$  unblock of NMDA receptors: implications for spike-timing dependent synaptic plasticity. *J Physiol* 556:337–345
- Karmarkar UR, Buonomano DV (2002) A model of spike timing dependent plasticity: one or two coincidence detectors? *J Neurosci* 22(11):507–513
- Koester HJ, Sakmann B (1998) Calcium dynamics in single spines during coincident pre- and postsynaptic activity depend on relative timing of back-propagating action potentials and subthreshold excitatory postsynaptic potentials. *PNAS* 95: 9596–9601
- Larkum ME, Kaiser KM, Sakmann B (1999) Calcium electrogenesis in distal apical dendrites of layer 5 pyramidal cells at a critical frequency of backpropagating action potentials. *PNAS* 96: 14600–14604
- Letzkus JJ, Kampa BM, Stuart GJ (2006) Learning rules for spike timing-dependent plasticity depend on dendritic synapse location. *J Neurosci* 26(41):10420–10429
- Lisman J (1997) Bursts as a unit of neural information: making unreliable synapses reliable. *TINS* 20(1):38–43
- Magee JC, Johnston D (1997) A synaptically controlled, associative signal for Hebbian plasticity in hippocampal neurons. *Science* 275:209–213
- Markram H, Luebke J, Frotscher M, Sakmann B (1997) Regulation of synaptic efficacy by coincidence of postsynaptic APs and EPSPs. *Science* 275:213–215
- Mayer ML, Westbrook GL, Guthrie BP (1984) Voltage-dependent block by  $Mg^{2+}$  of NMDA responses in spinal cord neurons. *Nature* 309:261–263
- Nevian T, Sakmann B (2004) Single spine  $Ca^{2+}$  signals evoked by coincident EPSPs and backpropagating action potentials in spiny stellate cells of layer 4 in the juvenile rat somatosensory barrel cortex. *J Neurosci* 24:1689–1699
- Nishiyama M, Hong K, Mikoshiba K, Poo MM, Kato K (2000) Calcium stores regulate the polarity and input specificity of synaptic modification. *Nature* 408:584–588
- Nishiyama M, Togashi K, Aihara T, Hong K (2010) GABAergic activities control spike timing- and frequency-dependent long-term depression at hippocampal excitatory synapses. *Front Syn Neurosci* 2(22):1–15
- Nowak L, Bregestovski P, Ascher P, Herbert A, Prochiantz A (1984) Magnesium gates glutamate-activated channels in mouse central neurons. *Nature* 307:462–465
- Otmakhova NA, Lisman JE (1999) Dopamine selectively inhibits the direct cortical pathway to the CA1 hippocampal region. *J Neurosci* 19:1437–1445
- Paulsen O, Li YG, Anderson P, Bliss TV (1993) Failure to induce long-term depression by an anti-correlation procedure in area CA1 of the rat hippocampal slice. *Eur J Neurosci* 5(10):1241–1246
- Pawlak V, Kerr JN (2008) Dopamine receptor activation is required for corticostriatal spike-timing-dependent plasticity. *J Neurosci* 28:2435–2446
- Poirazzi P, Brannon T, Mel BW (2003) Pyramidal neuron as a 2-layer neural network. *Neuron* 37:989–999
- Rubin JE, Gerkin RC, Bi GQ, Chow CC (2005) Calcium time course as a signal for spike-timing-dependent plasticity. *J Neurophysiol* 93:2600–2613
- Sabatini BL, Oertner TG, Svoboda K (2001)  $Ca^{2+}$  signalling in dendritic spines. *Curr Opin Neurobiol* 11(3):439–452
- Shimono K, Kubota D, Brucher F, Taketani M, Lynch G (2002) Asymmetrical distribution of the Schaffer projections within the apical dendrites of hippocampal CA1 field. *Brain Res* 950:279–287
- Shouval HZ, Bear MF, Cooper LN (2002) A unified model of NMDA receptor-dependent bidirectional synaptic plasticity. *Proc Natl Acad Sci USA* 99:10831–10836
- Sjostrom PJ, Turrigiano GG, Nelson SB (2001) Rate, timing, and cooperativity jointly determine cortical synaptic plasticity. *Neuron* 32:1149–1164
- Stent GS (1973) A physiological mechanism for Hebb's postulate of learning. *PNAS* 70(4):997–1001
- Stuart GJ, Hausser M (2001) Dendritic coincidence detection of EPSPs and action potentials. *Nat Neurosci* 4:63–71
- Stuart G, Schiller J, Sakmann B (1997) Action potential initiation and backpropagation in neurons of the mammalian CNS. *TINS* 20:125–131

- Tsukada M, Aihara T, Kobayashi Y, Shimazaki H (2005) Spatial analysis of spike-timing-dependent LTP and LTD in the CA1 area of hippocampal slices using optical imaging. *Hippocampus* 15:104–109
- Tzounopoulos T, Kim Y, Oerstel D, Trussell LO (2004) Cell-specific, spike timing-dependent plasticities in the dorsal cochlear nucleus. *Nat Neurosci* 7:719–725
- Vargas-Caballero M, Robinson HP (2003) A slow fraction of  $Mg^{2+}$  unblock of NMDA receptors limits their contribution to spike generation in cortical pyramidal neurons. *J Neurophysiol* 89: 2778–2783
- White JA, Banks MI, Pearce RA, Kopell NJ (2000) Networks of interneurons with fast and slow gamma-aminobutyric acid type A (GABAA) kinetics provide substrate for mixed gamma–theta rhythm. *PNAS* 97(10):8128–8133
- Whittington MA, Traub RD, Jeffreys JGR (1995) Synchronized oscillations in interneuron networks driven by metabotropic glutamate receptor activation. *Nature* 373:612–615
- Williams SR, Stuart GJ (1999) Mechanisms and consequences of action potential burst firing in rat neocortical pyramidal neurons. *J Physiol* 521:467–482
- Yao H, Dan Y (2001) Stimulus timing-dependent plasticity in cortical processing of orientation. *Neuron* 32:315–323
- Zhang LI, Tao HW, Holt CE, Harris WA, Poo M (1998) A critical window for cooperation and competition among developing retinotectal synapses. *Nature* 395:37–44